

# Stress granules sequester autophagy proteins to facilitate plant recovery from heat stress

---

Received: 2 February 2024

---

Accepted: 8 December 2024

---

Published online: 30 December 2024

---

 Check for updates

---

Xibao Li<sup>1,2,4</sup>, Jun Liao<sup>1,2,4</sup>, Ka Kit Chung<sup>1,3,4</sup>, Lei Feng<sup>1,2,4</sup>, Yanglan Liao<sup>1,2</sup>, Zhixin Yang<sup>1,2</sup>, Chuanliang Liu<sup>1,2</sup>, Jun Zhou<sup>1,2</sup>, Wenjin Shen<sup>1,2</sup>, Hongbo Li<sup>1,2</sup>, Chengwei Yang<sup>1,2</sup>, Xiaohong Zhuang<sup>3</sup> & Caiji Gao<sup>1,2</sup>✉

The autophagy pathway regulates the degradation of misfolded proteins caused by heat stress (HS) in the cytoplasm, thereby maintaining cellular homeostasis. Although previous studies have established that *autophagy* (*ATG*) genes are transcriptionally upregulated in response to HS, the precise regulation of ATG proteins at the subcellular level remains poorly understood. In this study, we provide compelling evidence for the translocation of key autophagy components, including the ATG1/ATG13 kinase complex (ATG1a, ATG13a), PI3K complex (ATG6, VPS34), and ATG8-PE system (ATG5), to HS-induced stress granules (SGs) in *Arabidopsis thaliana*. As HS subsides, SGs disassemble, leading to the re-translocation of ATG proteins back to the cytoplasm, thereby facilitating the rapid activation of autophagy to degrade HS-induced ubiquitinated aggregates. Notably, autophagy activation is delayed in the SG-deficient (*ubp1abc*) mutants during the HS recovery phase, resulting in an insufficient clearance of ubiquitinated insoluble proteins that arise due to HS. Collectively, this study uncovers a previously unknown function of SGs in regulating autophagy as a temporary repository for ATG proteins under HS and provides valuable insights into the cellular mechanisms that maintain protein homeostasis during stress.

Heat stress (HS) results in the buildup of misfolded proteins and damaged organelles in plant cells, thereby impairing plant growth and development<sup>1–4</sup>. The autophagy pathway plays a vital role in selectively removing these specific damaged components under such conditions<sup>5</sup>. Autophagy-deficient mutants often exhibit a hypersensitive phenotype to basal heat stress owing to the accumulation of ubiquitinated cargoes<sup>5–7</sup>. NBR1 (Next to BRCA1), the first identified autophagy receptor in plant<sup>8</sup>, has been shown to play a crucial role in autophagy-mediated removal of ubiquitinated misfolded proteins following HS<sup>5,9</sup>. NBR1 binds to K63-ubiquitinated substrates,

facilitating their removal by interacting with ATG8<sup>8</sup>. Although the transcriptional level of *autophagy* (*ATG*) genes is known to increase rapidly following HS<sup>6</sup>, there remains a lack of detailed research on the dynamic changes of these ATG proteins at subcellular levels during the HS and recovery phases.

Stress granules (SGs), which are transiently formed non-membrane-bound cellular compartments in the cytoplasm, function as reservoirs for mRNA and temporarily halt protein translation under stress conditions, facilitating translation recovery and promoting cell survival<sup>10,11</sup>. In plants, SGs can be induced by various abiotic stresses,

---

<sup>1</sup>Guangdong Provincial Key Laboratory of Biotechnology for Plant Development, School of Life Sciences, South China Normal University, Guangzhou, China.

<sup>2</sup>MOE Key Laboratory & Guangdong Provincial Key Laboratory of Laser Life Science, College of Biophotonics, South China Normal University, Guangzhou, China. <sup>3</sup>Centre for Cell & Developmental Biology and State Key Laboratory of Agrobiotechnology, School of Life Sciences, The Chinese University of Hong Kong, Hong Kong, China. <sup>4</sup>These authors contributed equally: Xibao Li, Jun Liao, Ka Kit Chung, Lei Feng. ✉e-mail: [gaocaiji@m.scnu.edu.cn](mailto:gaocaiji@m.scnu.edu.cn)

such as hypoxia, oxidative phosphorylation inhibitors, osmotic, drought, and heat stresses<sup>1–17</sup>. In addition, the plant hormones salicylic acid (SA) and abscisic acid (ABA) can trigger the formation of SGs<sup>18,19</sup>. SGs assembly-deficiency mutants frequently exhibit a phenotype of hypersensitivity to abiotic stresses<sup>13,17,20,21</sup>. SGs primarily consist of translation initiation factors, RNA-binding proteins, and mRNAs that are stalled during translation initiation. However, non-RNA-binding proteins have also been found in SGs, implying their involvement in functions other than mRNA protection<sup>22</sup>. In mammals and yeast, Raptor, a component of the target of rapamycin complex 1 (TORC1), is recruited from the vacuolar membrane to SGs during HS, thereby sequestering TORC1 signaling<sup>23,24</sup>, as is the case with other signaling molecules including JUN, RACK1, and TRAF2<sup>25–27</sup>. In *Arabidopsis*, TSN1 and TSN2 facilitate the recruitment of SnRK1 to SGs, serving as a docking platform for SnRK1 activation during HS<sup>28</sup>. Other stress-related kinases, such as MPK3, MKK5, and CDKA;1, are also localized in HS-induced SGs<sup>22</sup>. These studies suggest that SGs not only protect mRNA but also play a role in sequestering signaling molecules and protecting proteins during unfavorable conditions.

Here, we discovered that specific key ATG proteins formed punctate signals during HS at 38 °C. Moreover, these punctate signals exhibited colocalization with non-membranous organelle SGs, but not with membranous organelles. As HS subsides, ATG proteins retranslocate from SGs to the cytoplasm, rapidly activating autophagy to degrade ubiquitinated insoluble protein aggregates in *Arabidopsis*. This study revealed the role of SGs in regulating plant autophagy during HS.

## Results

### Autophagy-related proteins accumulate to SGs after heat treatment

Recently, we reported that ATG8 translocated to the swollen Golgi membrane to facilitate Golgi reassembly after short-term acute HS<sup>29</sup>. To comprehensively examine the responses of core ATG proteins to HS, we performed heat treatment on a collection of *Arabidopsis* transgenic lines stably expressing fluorescent protein-tagged ATG proteins. The transgenic lines were subjected to HS treatment at 38 °C for 1 h, followed by confocal observation of fluorescent signals. The obtained results revealed that ATG8 proteins did not exhibit an obvious accumulation of punctate upon treatment at 38 °C for 1 h (Fig. 1a), which contrasts with the observed accumulation of ATG8 in the Golgi apparatus following treatment at 45 °C<sup>29</sup>. Surprisingly, we found that other ATG proteins, including the ATG1/ATG13 kinase complex (ATG1a, ATG13a), PI3K complex (ATG6, VPS34), and ATG12-ATG5 ubiquitination-like system (ATG5), formed aggregate-like punctate structures after HS at 38 °C for 1 h (Fig. 1a). This observation revealed a previously unrecognized localization pattern of ATG proteins under HS, and we therefore fixed the treatment condition as 1 h HS at 38 °C in the following experiments. HS-induced punctate formation of ATG proteins was observed in both root and cotyledon cells (Supplementary Fig. 1). Additionally, we noticed that some ATG members, including ATG3-GFP, ATG7-GFP, ATG18a-GFP, and ATG9-GFP, did not show obvious changes in their localization pattern upon HS (Fig. 1a).

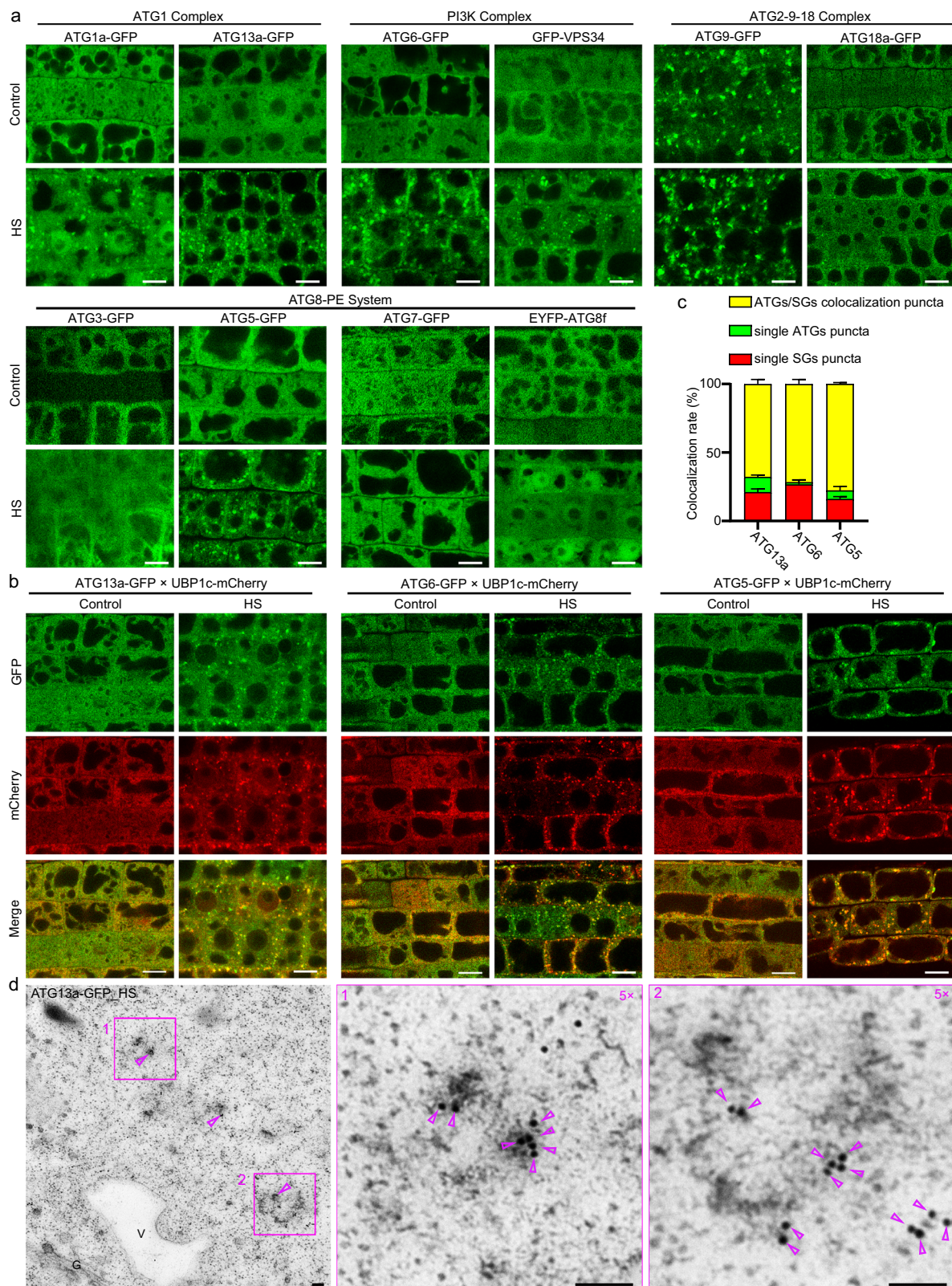
To determine the precise subcellular localization of HS-induced ATG puncta, we crossed these fluorescent-tagged ATG lines with various organelle markers, including the *cis*-Golgi apparatus marker mRFP-SYP32, *trans*-Golgi network (TGN) marker VHAa1-mRFP, multivesicular endosome marker mRFP-Rha1, and mitochondria marker Mito-mRFP. However, HS-induced ATG puncta did not exhibit obvious colocalization with these typical membranous organelles (Supplementary Figs. 2 and 3). This observation motivated us to speculate on the localization of these ATG proteins to membraneless organelles upon HS. One common type of membraneless organelle transiently formed under HS is SGs, which can be specifically labeled by core SG

components such as UBPIc and Rbp47b<sup>14,17,20,21,28</sup>. Therefore, we created double transgenic lines co-expressing ATG-GFP fusions and UBPIc-mCherry for subcellular localization analysis. In line with our expectations, HS-induced ATG puncta exhibited perfect colocalization with the SGs marker UBPIc-mCherry on punctate structures following HS (Fig. 1b, c). To closely examine the ultrastructure of ATG protein-localized puncta, we next performed immuno-transmission electron microscopy (TEM) using GFP antibodies on ultrathin sections prepared from high-pressure frozen/freeze-substituted roots of HS-treated ATG13a-GFP line. The TEM results revealed that the gold particles were frequently concentrated in electron-dense areas with irregular shapes (Fig. 1d), whose morphology resembles that of SGs shown in previous reports<sup>30</sup>. ATG9, the only transmembrane protein in the autophagy pathway<sup>31</sup>, exhibited a punctate signal both before and after HS (Fig. 1a), but neither ATG9 nor its associated protein ATG18a appeared to localize on HS-induced SGs (Supplementary Fig. 4a, b). Moreover, it is known from previous reports that 34 °C represents the minimum threshold temperature for SG formation in *Arabidopsis*, and as the temperature increases, both the formation rate and the number of SGs significantly increase<sup>30</sup>. Therefore, we examined the localization patterns of SGs and ATG protein aggregates induced by HS at various temperatures. Upon HS at 34 °C for 1 h, while ATG protein aggregates and SGs began to appear in the cytoplasm, their co-localization was minimal (Supplementary Fig. 4c, f). However, as the temperature rises, the co-localization of ATG proteins and SGs gradually increases (Fig. 1b, c and Supplementary Fig. 4c–h), indicating a stronger association of ATG proteins and SGs within the temperature range of 38–40 °C. Unfortunately, stimulation at higher temperatures at 42 °C to 45 °C for 1 h led to cell death of these seedlings, thereby precluding further investigation at higher temperatures. Collectively, these results definitively established a link between autophagy machinery and SGs in plants and clearly demonstrated the incorporation of some key ATG proteins belonging to the ATG1/ATG13 kinase complex, PI3K complex, and ATG12-ATG5 ubiquitin-like conjugation system into SGs during a primed HS at 38–40 °C for 1 h.

### ATG proteins associate with SGs components in vivo under heat treatment

During the non-stress phase, the core components of SGs can establish a pre-interaction network, allowing the quick assembly of SGs in response to stresses<sup>32,33</sup>. We also observed the existence of this pre-interaction network, as evidenced by the detection of UBPIa and RBP47b interactions under normal growth conditions (Supplementary Fig. 5a). To test whether ATG proteins were present in this pre-interaction network, we performed bimolecular fluorescence complementation (BiFC) and co-immunoprecipitation (Co-IP) assays to test the possible associations between ATG proteins and SGs components. Under normal growth conditions, no BiFC signals were detected between ATG13a-YN, ATG1a-YN, YN-ATG6, YN-VPS34, ATG5-YN, and UBPIa-YC (Fig. 2a and Supplementary Fig. 5b, c), indicating that ATG proteins (ATG13a, ATG1a, ATG6, VPS34, and ATG5) are not present in the pre-interaction network of SGs components. Upon HS, a significant number of punctate BiFC signals were detected, colocalizing with SGs markers (Fig. 2a and Supplementary Fig. 5b, c), while negative controls showed no BiFC signals, irrespective of HS treatment (Supplementary Fig. 6). The associations between ATG proteins and SGs components were further corroborated by Co-IP assays, in which UBPIa-GFP precipitated ATG13a-FLAG, ATG6-FLAG, and ATG5-FLAG only under HS conditions (Fig. 2b–d). The above results suggest that ATG proteins (ATG13a, ATG1a, ATG6, VPS34, and ATG5) are recruited to SGs induced by HS, but do not exist in the pre-interaction network of SGs under normal conditions.

Next, we applied a modified approach of differential centrifugation to isolate SGs from plant cells to determine the potential coexistence of ATG proteins and SGs components in the same cellular



compartments (Fig. 2e)<sup>22</sup>. Initially, we expressed two distinct SGs markers, UBP1a-GFP and mCherry-RBP47b, in *Arabidopsis* protoplasts to evaluate the feasibility of our method in SGs isolation. The obtained results demonstrated that this approach effectively separated aggregates co-labeled with both SGs markers (Fig. 2f). Subsequently, we obtained cell lysis of *Arabidopsis* cells with co-expression of ATG-GFP and the SGs marker UBP1a-FLAG or mCherry-RBP47b with or without

HS treatment, followed by separation of the SGs-free and SGs-containing fractions in the supernatant and precipitate, respectively. Firstly, the suspended precipitates were examined using confocal microscope, revealing a high degree of co-localization between the ATG proteins (ATG13a, ATG1a, ATG6, VPS34, ATG5) and mCherry-RBP47b on the puncta within the isolated SGs-enriched fraction (Fig. 2g and Supplementary Fig. 7). Subsequently, we performed

**Fig. 1 | Autophagy-related proteins accumulate on SGs after heat treatment.**  
**a** The 5-day-old transgenic plants expressing GFP fusions of ATG proteins, including the ATG1 complex (ATG1a-GFP, and ATG13a-GFP), PI3K complex (ATG6-GFP, and GFP-VPS34), ATG2-9-18 complex (ATG9-GFP, and ATG18a-GFP), and ATG8-PE system (ATG3-GFP, ATG5-GFP, ATG7-GFP, and EYFP-ATG8f), were subjected to treatment at 22 °C (control) or 38 °C (HS) for 1 h. The Meristem zone of indicated samples was observed using a confocal microscope. Scale bar = 10  $\mu$ m. **b** The 5-day-old plants expressing ATG13a-GFP  $\times$  UBPI1c-mCherry, ATG6-GFP  $\times$  UBPI1c-mCherry, ATG5-GFP  $\times$  UBPI1c-mCherry were subjected to treatment at 22 °C (control) or 38 °C

(HS) for 1 h. The Meristem zone of indicated samples was observed using a confocal microscope. UBPI1c-mCherry serves as SGs marker. Scale bar = 10  $\mu$ m. **c** Co-localization analysis of ATG proteins puncta with SGs after 38 °C HS in **(b)**. Data represent mean  $\pm$  SD,  $n = 5$ . Five different 50  $\times$  50  $\mu$ m<sup>2</sup> areas in the meristem zone were used for colocalization analysis. **d** Transmission electron micrographs (TEM) of ATG13a-GFP plant after HS treatment at 38 °C for 1 h. Immuno-gold labeling with GFP antibody showing the location of ATG13a-GFP. The magenta arrowheads indicate the GFP-antibody-coated gold particles. Scale bar = 100 nm. G: Golgi apparatus. V: vacuole. Source data are provided as a Source Data file.

immunoblotting to assess the distribution of ATG proteins and UBPI1a-FLAG across the SGs-free supernatant and SGs-containing precipitate fractions. Under normal conditions, both ATG proteins and UBPI1a-FLAG were detected in the supernatant, with no presence in the precipitate (Fig. 2h and Supplementary Fig. 8). In contrast, following HS treatment, there was a pronounced accumulation of ATG proteins and UBPI1a-FLAG in the precipitate, while their levels in the supernatant were notably reduced (Fig. 2h and Supplementary Fig. 8). In line with our expectations, ATG8f and ATG3, which failed to translocate to the SGs (Fig. 1a), were not present in the precipitate upon HS (Supplementary Fig. 8c). In conclusion, these findings strongly suggest an *in vivo* association between ATG proteins and SGs components under HS conditions, leading to their co-precipitation in cell lysates.

### The translocation of ATG protein to SGs depends on the assembly of SGs under HS

We proceeded to assess the impact of SG disruption on ATGs punctate accumulation during HS and to explore the possible presence of ATG proteins in SGs induced by conditions other than HS. CHX (cycloheximide), a drug that binds to ribosome small subunits to inhibit translation, is known to be a potent inhibitor of SG formation under HS and other stress conditions<sup>17,34</sup>. As expected, CHX treatment inhibited the formation of HS-induced ATG puncta and SGs (Fig. 3a and Supplementary Fig. 9a). We also examined the effects of other stressors, such as osmotic, salt, drought, and oxidative stress induced by arsenite, on the distribution of ATG proteins. While these stressors are recognized for robustly triggering SGs formation in plants<sup>11-17,35</sup>, they did not influence the distribution of ATG proteins (Supplementary Fig. 9b). Collectively, these observations suggest that the translocation of ATG proteins to SGs relies on SG assembly induced by HS, but not by other stress conditions as mentioned above.

In *Arabidopsis*, the triple RNA recognition motif (RRM) OLIGOURIDYLATE BINDING PROTEIN 1 family proteins (UBPI1a, UBPI1b, and UBPI1c) are homologous to mammalian TIA1 and TIAR, serving as core components in SG assembly<sup>17,35,36</sup>. To test the dependence of SG assembly on the translocation of ATG proteins to SGs, we obtained a *ubp1abc* triple null mutant by introducing the *ubp1c-cas9* mutation edited by CRISPR/Cas9 technology into the *ubp1a-1* and *ubp1b-1* T-DNA insertion mutants (Supplementary Fig. 16a-d). Consistent with the effects observed in *TIA1/TIAR* knockout cell line<sup>36</sup>, the *ubp1abc* triple mutant showed an obvious reduction in the number of SGs during HS (Supplementary Fig. 16e, f). Subsequently, we selected ATG13a, ATG6, and ATG5 as representatives of various autophagy regulatory complexes and obtained transgenic lines with expression of their GFP fusions in the *ubp1abc* triple mutant. We noticed that the number of puncta corresponding to GFP fusions of these ATG proteins decreased significantly in *ubp1abc* triple mutant compared to that in WT plants after 1 h of HS (Fig. 3b, c), while their protein expression levels remained similar (Supplementary Fig. S16h-j). These results suggest the dependence of SGs assembly for the translocation of ATGs proteins to punctate structures during the HS phase.

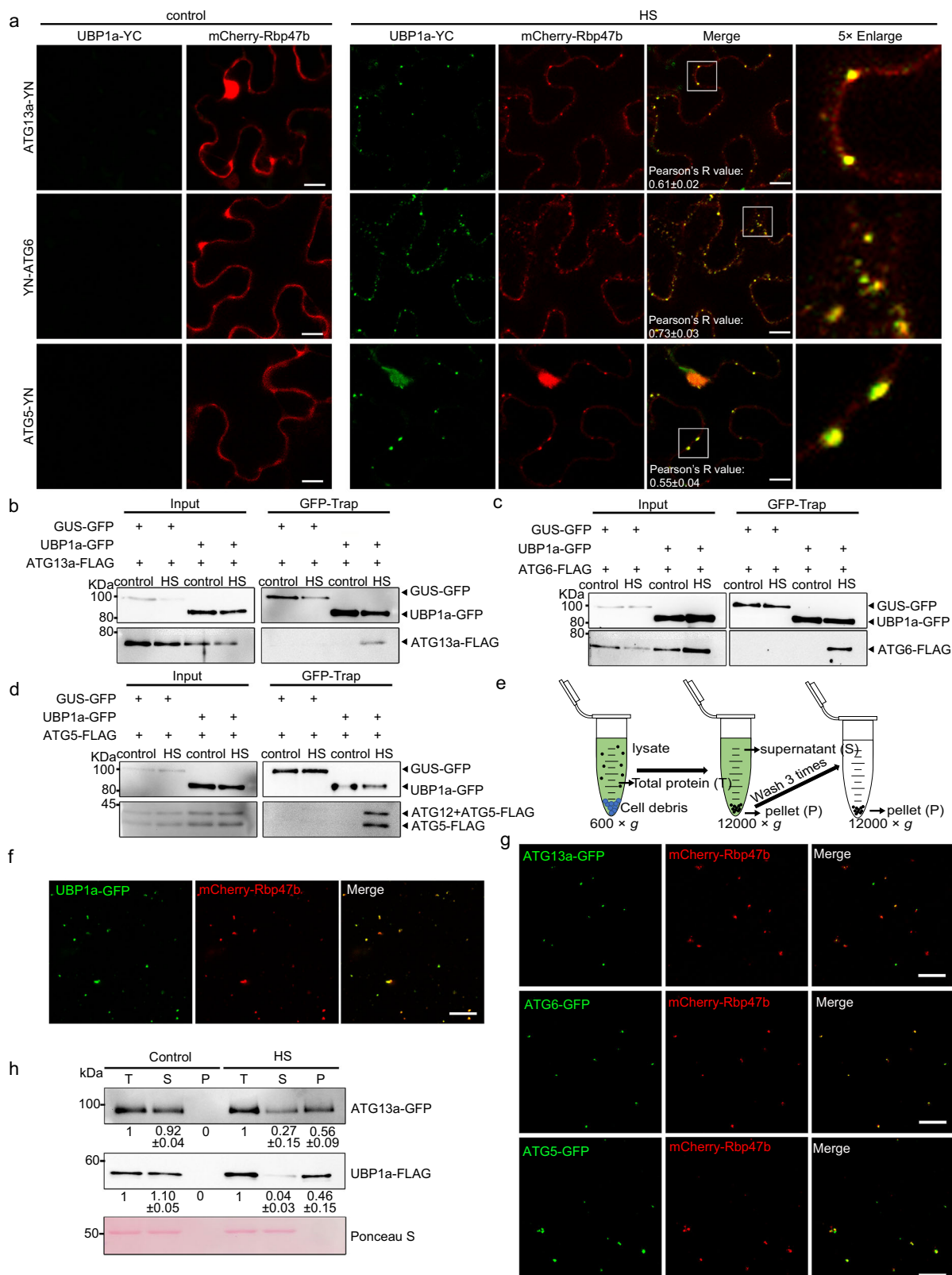
Following recovery from HS to normal conditions, SGs undergo disassembly within a few hours, allowing for the release of their contents into the cytoplasm and facilitating rapid recovery of cellular

processes<sup>10</sup>. Despite the presence of ATG proteins within SGs, no significant difference was observed in the assembly and disassembly of SGs between wild-type and *atg5-1* mutant plants following HS treatment (Fig. 3d, e). This suggests that ATG proteins are not essential for SGs assembly and disassembly under plant HS conditions, which is consistent with the observation of autophagy-independent clearance of HS-induced SGs in mammalian cells<sup>37,38</sup>. Next, we tested the dynamics of ATG proteins upon SGs disassembly during the recovery phase. As shown in Fig. 3d, e, the number of SGs gradually decreased and almost completely disappeared at 6 h recovery from HS. Concurrently, the punctate signals of ATG13a, ATG6, and ATG5 disappeared at 6 h recovery from HS (Fig. 3f and Supplementary Fig. 10). In summary, these findings provide insights into the dynamic regulation of the subcellular localization of ATG proteins (ATG13a, ATG1a, ATG6, VPS34, and ATG5) during HS and recovery period, highlighting their connections with SGs.

### Autophagy is activated during the HS recovery phase

The dynamic incorporation and release of ATG proteins from SGs led us to hypothesize that the sequestration of ATG proteins into SGs suppresses autophagy during HS, while their subsequent release enables rapid activation of autophagy during the recovery stage. To test this hypothesis, we monitored the formation of autophagosomes labeled with EYFP-ATG8f during the time-lapse of the HS recovery stage. To this end, the EYFP-ATG8f seedlings were subjected to HS at 38 °C for 1 h, followed by recovery at 22 °C and subsequent observation at various time points. The EYFP-ATG8f-labeled puncta in cytoplasm and autophagosomes inside vacuoles were rarely observed during the 1 h HS period (Fig. 4a and Supplementary Fig. 11b), indicating the inhibition of autophagosome formation at this stage, which is consistent with previous studies highlighting the inhibition of autophagy activity during the period of HS<sup>39</sup>. However, during the recovery phase, EYFP-ATG8f rapidly formed numerous punctate structures (Fig. 4a), emerging as early as 1 h after recovery, reaching a peak at 6 h, followed by a gradual decline (Fig. 4b). This puncta formation was not exclusive to ATG8f, as other ATG8 isoforms (ATG8a, ATG8b, ATG8d, ATG8h) were also seen to form punctate structures, regardless of their fluorescent tags (Supplementary Fig. 11a). Notably, most of the puncta labeled by EYFP-ATG8f initially appeared as solid structures during the first 6 h of recovery, transitioning to more circular autophagosome-like structures at 9 h post-recovery (Fig. 4a). Ultimately, most circular autophagosomes disappeared at 12 h after HS recovery (Fig. 4a, b).

To validate whether these puncta labeled with EYFP-ATG8f represent autophagosomes, we conducted immuno-gold-TEM using GFP antibodies on ultrathin sections prepared from high-pressure frozen/freeze-substituted roots of EYFP-ATG8f plants at 3 and 9 h post-HS recovery. As shown in Fig. 4c and Supplementary Fig. 12, the labeling of anti-GFP gold particles was predominantly found on electron-dense condensates at 3 h, with occasional detection on cup-shaped phagophores, suggesting the recognition of protein aggregates by ATG8 and the initiation of autophagosome formation at this stage. TEM imaging also revealed a scarcity of double-membrane autophagosomes during the early recovery stage (Fig. 4c and



Supplementary Fig. 12a). In contrast, the labeling of double-membrane autophagosomes with gold particles was easily discernible at 9 h post-recovery (Fig. 4c and Supplementary Fig. 12b), aligning with the confocal microscopy observations of circular structures (Fig. 4a). The disappearance of most EYFP-ATG8f puncta by 12 h post-recovery indicates the delivery of EYFP-ATG8f autophagic vesicles into vacuoles for degradation. To further assess the autophagy activity, we treated

HS-primed plants with Concanamycin A (Conc A), an inhibitor of vacuolar H<sup>+</sup>-ATPase<sup>40,41</sup>, to visualize the autophagic bodies inside vacuoles. The obtained results demonstrated that the EYFP-ATG8f-labeled autophagic bodies inside vacuoles were barely detectable during the first 3 h of recovery, with only a few observed at 6 h post-recovery (Fig. 4d, e). However, a significant number of autophagic bodies inside vacuoles could be clearly observed at 9 and 12 h post-

**Fig. 2 | ATG proteins associate with SGs components in vivo under HS.** **a** BiFC assays demonstrate the association of ATG proteins and UBPI1a in vivo under HS. ATG13a-YN, ATG6-YN, ATG5-YN, and UBPI1a-YC were co-expressed in tobacco leaves. mCherry-RBP47b was co-expressed as SGs marker. For HS treatment, the isolated tobacco leaves were placed in a 38 °C incubator for 1 h. Scale bar = 10  $\mu$ m. The value represents the Pearson Correlation Coefficient. Data represent mean  $\pm$  SEM,  $n = 3$ . Three different merged images are used for the calculation. **b–d** Co-IP assays demonstrate associations between ATG proteins and SGs components (UBPI1a) in planta. Total proteins were extracted from plant cells co-expressing GUS-GFP/ATG-FLAG and UBPI1a-GFP/ATG-FLAG with 22 °C (control) and 38 °C (HS) treatment, followed by immunoprecipitation using GFP-Trap magnetic beads. The immunoprecipitated protein was detected by WB using anti-GFP or anti-FLAG antibody. **e** Schematic diagram of separate SGs by differential centrifugal method.

**f, g** *Arabidopsis* cells co-expressing mCherry-RBP47b and UBPI1a-GFP, ATG13a-GFP, ATG6-GFP or ATG5-GFP were subjected to HS treatment at 38 °C for 1 h, followed by differential centrifugation to separate SGs. Precipitate was resuspended in a few of the wash buffers, followed by observation using confocal microscopy. Scale bar = 10  $\mu$ m. **h** *Arabidopsis* cells co-expressing UBPI1a-FLAG/ATG13a-GFP were subjected to treatment at 22 °C (control) or 38 °C (HS) for 1 h, followed by differential centrifugation to separate SGs. An equal proportion of denatured samples (T: total protein, S: supernatant, P: pellet) were separated by 10% SDS-PAGE, followed by immunoblotting with anti-GFP, and anti-FLAG antibodies. Ponceau staining represents the Rubisco large subunit, which was used as the reference for loading control. The value represents the S or P vs. T. Data represent mean  $\pm$  SEM;  $n = 2$ . Source data are provided as a Source Data file.

recovery (Fig. 4d, e). These findings imply a correlation between the temporal regulation of autophagosome formation and the dynamics of assembly and disassembly of ATG-containing SGs. It is likely that the substantial sequestration of ATG proteins in SGs during HS impeded the initiation of autophagy, while their subsequent release during the recovery phase promoted the autophagy process.

### ATG8-labeled puncta co-localizes with NBRI-decorated particles during the HS recovery phase

In mammalian cells, the autophagy pathway is involved in the clearance of persistent SGs resulting from prolonged stress or disease mutations, but it does not participate in the disassembly of transiently formed SGs<sup>37,38</sup>. To explore whether ATG8-labeled puncta colocalize with SGs undergoing disassembly during the HS recovery in plants, we crossed the UBPI1c-GFP and mCherry-ATG8f plants to generate double transgenic lines for HS treatment and confocal observation. However, we did not observe any colocalization between the EYFP-ATG8f-labeled puncta and the disassembling SGs at 3 h post-HS recovery (Fig. 5a). This lack of colocalization suggests that these ATG8f-labeled puncta might not be involved in the clearance of HS-induced SGs, aligning with the finding that disassembly of SGs remains unaffected in the *atg5-1* mutant (Fig. 3d, e).

The ATG8-interacting protein NBRI has been identified as an autophagy receptor, which binds to ubiquitinated proteins and mediates the clearance of HS-induced protein aggregates by autophagy<sup>5,9,39</sup>. To validate whether EYFP-ATG8f-labeled puncta colocalized with NBRI-decorated cytoplasmic puncta during the HS recovery phase, we obtained the double transgenic plants co-expressing NBRI-GFP and mCherry-ATG8f and subjected them to HS treatment. Remarkably, after HS for 1 h, numerous NBRI aggregates appeared in the cytoplasm, whereas ATG8 did not exhibit significant accumulation on punctate structures (Fig. 5b). As recovery progressed, ATG8 gradually accumulated on these NBRI aggregates (Fig. 5b, c), indicating that ATG8 began to recognize these NBRI-decorated protein aggregates during the recovery phase. By 9 h post-HS recovery, some NBRI-GFP puncta appeared on the circular autophagosomes decorated with mCherry-ATG8f (Fig. 5d). After treatment with Conc A, the puncta co-labeled with NBRI-GFP and mCherry-ATG8f were easily detected inside vacuoles, whereas the HS-primed plants accumulated substantially more puncta when compared to untreated plants (Fig. 5e, f). Collectively, these results suggest the boost of autophagy activity during recovery from HS, which likely aids in the clearance of protein aggregates marked by NBRI.

### Autophagy activation is slowed in SG-deficiency (*ubp1abc*) mutants during the HS recovery phase

The above results suggest that SGs may transiently sequester ATG proteins during the HS phase, and their release during the HS recovery phase facilitates the timely activation of autophagy, which possibly helps enhance plant resilience to heat stress. Failure in SGs assembly could potentially lead to differences in the activation of autophagy

compared to the WT during the HS recovery phase. To test this hypothesis, we introduced EYFP-ATG8f into the *ubp1abc* triple mutant background for evaluating autophagy activity. Initially, we examined the localization of EYFP-ATG8f during the recovery phase and found that although the EYFP-ATG8f condensates were still formed in the *ubp1abc* mutant at the early stage of HS recovery (before 6 h), the appearance of circular autophagosomes labeled by EYFP-ATG8f was obviously delayed in comparison to WT plants (Fig. 6a, b). Under conditions of carbon starvation, both *ubp1abc* and WT plants exhibited similar levels of EYFP-ATG8f-labeled autophagic bodies within vacuoles (Supplementary Fig. 13), indicating that the *ubp1abc* mutation does not affect the general autophagy activation induced by energy deficit. However, when subjected to Conc A treatment after HS, the *ubp1abc* mutant showed a significantly reduced accumulation of autophagic bodies within vacuoles compared to WT plants at 9- and 12-h post-HS recovery (Fig. 6c, d), suggesting a delay in the activation of autophagy in the *ubp1abc* mutant during the HS recovery phase. To substantiate this conclusion, we performed immunoblotting with anti-ATG8 antibodies to analyze the lipidated and non-lipidated forms of ATG8. The lipidated ATG8 (ATG8-PE adduct) mainly labels the forming autophagic vesicles and completed autophagosomes, and the ratio of ATG8-PE to ATG8 is indicative of autophagy activity<sup>42</sup>. The obtained results showed that the ATG8-PE adduct appeared during the post-HS recovery period, whereas the ATG8-PE/ATG8 ratio was substantially lower in *ubp1abc* mutant than in WT plants (Supplementary Fig. 14), suggesting reduced autophagy activity in this mutant.

Given that HS causes a sharp increase in ubiquitinated insoluble proteins, and considering that autophagy is known to assist in their elimination<sup>5</sup>, we hypothesized that delayed activation of autophagy might result in insufficient clearance of ubiquitinated insoluble proteins in SG-deficiency mutant. To test this hypothesis, we initially quantified the protein levels of NBRI and ATG8 in both WT and *ubp1abc* mutants during the HS and subsequent recovery phases. The obtained results revealed a pronounced accumulation of NBRI and ATG8 in the *ubp1abc* mutant compared to the WT, particularly during the recovery phase following HS (Fig. 6e). Subsequently, we examined the abundance of ubiquitinated insoluble proteins in the WT and *ubp1abc* mutants across the HS and recovery periods. As expected, the ubiquitinated insoluble protein increased markedly after HS and did not decrease significantly within the first 6 h of recovery, but showed a significant reduction after 12 h of recovery (Fig. 6f and Supplementary Fig. 15). This aligns with the appearance of circular autophagosomes and the accumulation of autophagic bodies at 9–12 h post-HS recovery (Fig. 4). Notably, the results showed that the enrichment of ubiquitinated insoluble proteins was significantly higher in the *ubp1abc* mutants than the WT seedlings at 12 h following HS recovery (Fig. 6f, g and Supplementary Fig. 15). Collectively, these findings suggest that disruption of SG assembly leads to a delay in autophagy activation and inadequate clearance of HS-induced ubiquitinated insoluble protein aggregates during HS recovery phase.

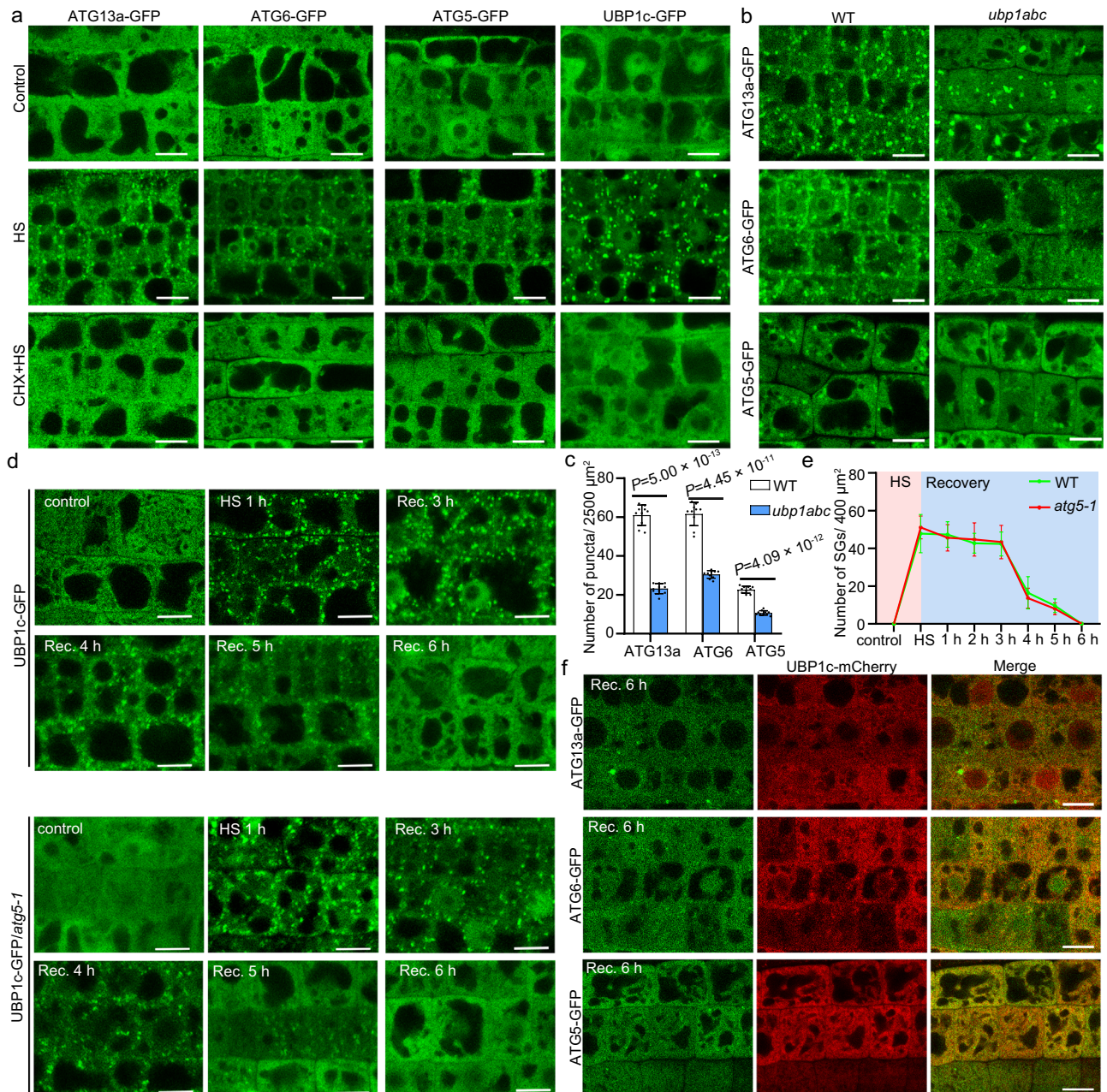


**Fig. 3 | Translocation of ATG proteins to SGs depends on the assembly of SGs under HS.** **a** The 5-day-old ATG13a-GFP, ATG6-GFP, ATG5-GFP, and UBPIc-GFP plant were subjected to 22 °C (control), 38 °C (HS) or 50  $\mu\text{M}$  CHX + 38 °C HS treatment for 1 h. The root tips of indicated samples were observed using a confocal microscope. Scale bar = 10  $\mu\text{m}$ . **b** The 5-day-old transgenic plants expressing ATG13a-GFP, ATG6-GFP, or ATG5-GFP in either WT or *ubp1abc* mutant were subjected to HS treatment at 38 °C for 1 h. The Meristem zone of indicated samples was observed using a confocal microscope. Scale bar = 10  $\mu\text{m}$ . **c** Statistical analysis of the number of foci signals in **(b)**. Data represent mean  $\pm$  SD;  $n = 10$ . Ten different  $50 \times 50 \mu\text{m}^2$  areas in the meristem zone were used for colocalization analysis. Statistical analysis was performed using a two-tailed unpaired Student's *t* test. **d** The

UBPIc-GFP and UBPIc-GFP/*atg5-1* plants were subjected to treatment at 22 °C (control) or 38 °C (HS) for 1 h, followed by heat-stressed plants recovered at 22 °C. The Meristem zone of indicated samples was observed using a confocal microscope. Scale bar = 10  $\mu\text{m}$ . **e** Statistical analysis of the number of SG in WT and *atg5-1* at HS and HS recovery phase in **(d)**. Data represent mean  $\pm$  SD;  $n = 8$ . Eight different  $20 \times 20 \mu\text{m}^2$  areas in the meristem zone were used for colocalization analysis. **f** The 5-day-old ATG-GFP  $\times$  UBPIc-mCherry plants were subjected to HS treatment at 38 °C for 1 h, followed by recovery at 22 °C for 6 h. The Meristem zone of indicated samples was observed using a confocal microscope. Scale bar = 10  $\mu\text{m}$ . Source data are provided as a Source Data file.

## Discussion

Autophagy is a conserved cellular process that occurs at a basal level in plants under normal conditions, while it can be triggered to enhance plant resilience when faced with disadvantages, such as nutritional deficiency, salt stress, or temperature fluctuations<sup>43–51</sup>. In this study, we uncovered a novel regulatory mechanism for autophagy in response to HS in *Arabidopsis*. Our study demonstrates that key ATG proteins

undergo rapid translocation to SGs, thereby temporarily inhibiting autophagy during the HS phase. Upon recovery from HS, these ATG proteins re-translocate to the cytoplasm accompanying SGs disassembly, thereby activating autophagy to facilitate the clearance of ubiquitinated insoluble protein aggregates that accumulate during HS (Fig. 7). In summary, we elucidated a novel subcellular process of ATG protein mobilization that regulates autophagy activity in response to

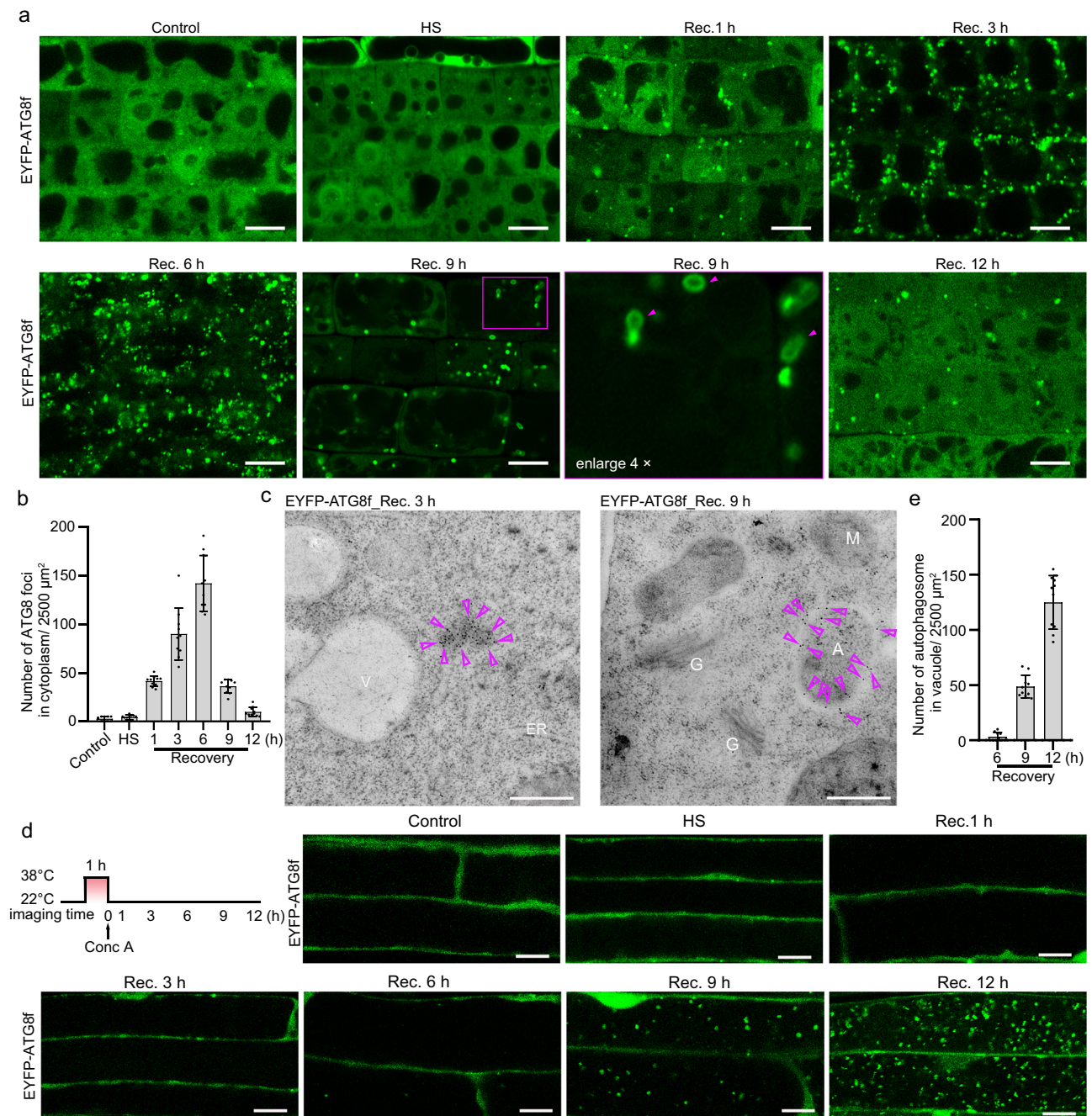


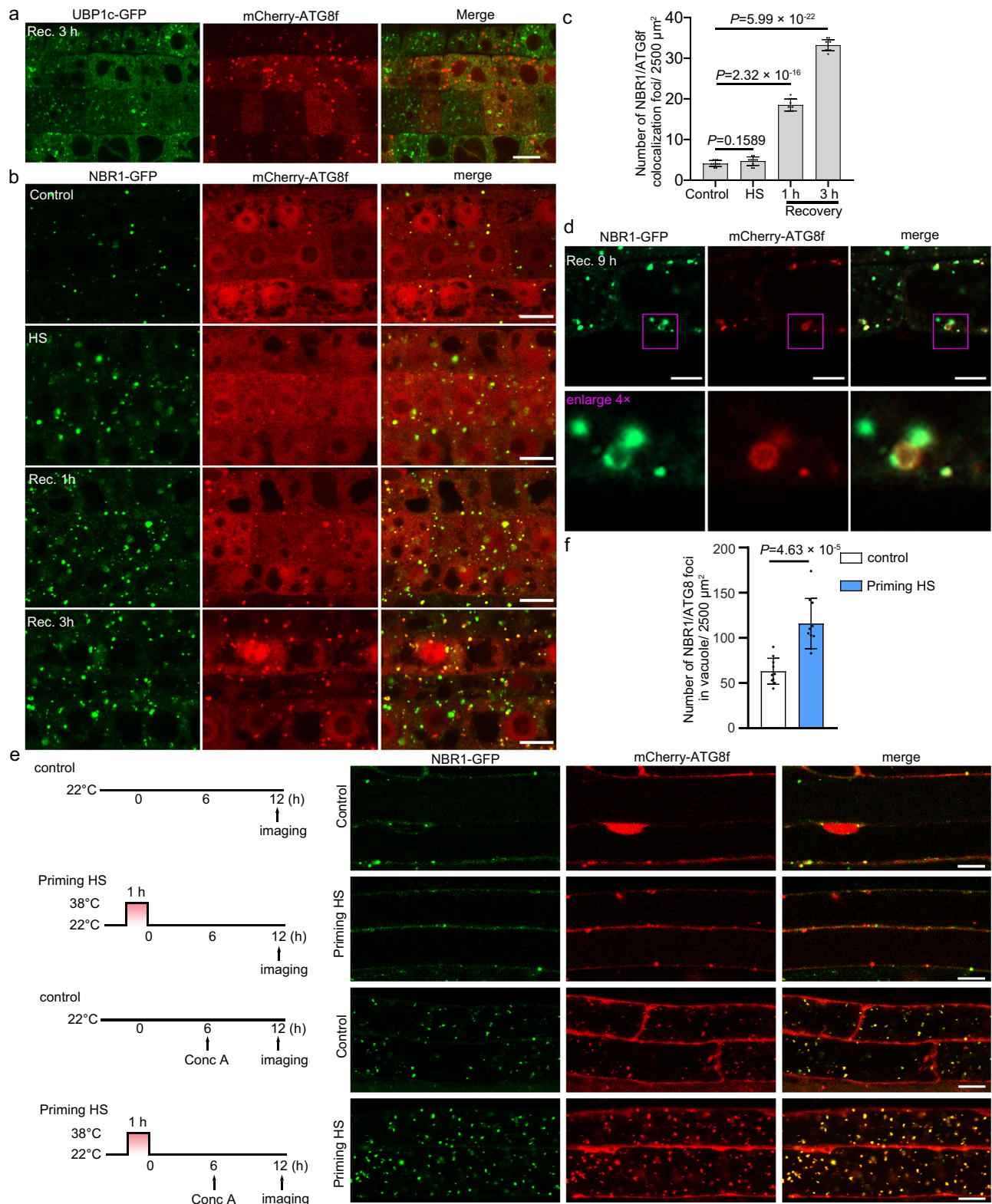
**Fig. 4 | Autophagy is activated during the HS recovery phase.** **a** The 5-day-old EYFP-ATG8f plants were subjected to treatment at 22 °C (control) or 38 °C (HS) for 1 h, followed by heat-stressed plants recovered at 22 °C for 1 h, 3 h, 6 h, 9 h, and 12 h. The Meristem zone of indicated samples was observed using a confocal microscope. Scale bar = 10 μm. **b** Statistical analysis of the number of foci signals in (a). Data represent mean ± SD;  $n = 10$ . Ten different  $50 \times 50 \mu\text{m}^2$  areas in the meristem zone were used for colocalization analysis. **c** TEM images of the EYFP-ATG8f plant during the recovery phase. EYFP-ATG8f plants were subjected to HS treatment at 38 °C for 1 h, followed by recovery at 22 °C for 3 h or 9 h. Immuno-gold labeling with GFP antibody showing the location of EYFP-ATG8f. The magenta arrowheads

indicate the GFP-antibody-coated gold particles. Scale bar = 500 nm. A, autophagosome; ER, endoplasmic reticulum; G, Golgi apparatus; M, mitochondria; V, vacuole. **d** The 5-day-old EYFP-ATG8f plants were subjected to treatment at 22 °C (control) or 38 °C (HS) for 1 h, followed by heat-stressed plants recovered at 1/2 MS liquid medium supplemented with 1 μM Conc A for 1 h, 3 h, 6 h, 9 h, and 12 h at 22 °C. The maturation zone of the roots from the indicated samples was observed using a confocal microscope. Scale bar = 10 μm. **e** Statistical analysis of the number of autophagosomes in the vacuole in (d). Data represent mean ± SD;  $n = 10$ . Ten different  $50 \times 50 \mu\text{m}^2$  areas in the maturation zone were used for analysis. Source data are provided as a Source Data file.

HS. These findings enhance our understanding of cellular stress responses and highlight the important roles of SGs in plant responses to HS.

Here, we observed that certain ATG proteins aggregated into SGs after HS (Fig. 1) and that the formation of ATG puncta depended on SGs assembly (Fig. 3). A key question is how these ATG proteins are

recruited to the SGs. The scaffold-client model has been employed to elucidate the role of core components (scaffold proteins, essential for SGs formation) and client components (biomolecules recruited via scaffold-client interactions) in SGs formation within mammalian and yeast cells<sup>36,52–54</sup>. SG assembly is driven by oligomerization and phase separation of scaffold proteins to form a scaffold–scaffold–RNA bond



network<sup>36</sup>. Subsequently, client proteins are recruited to scaffold–scaffold binding sites. Despite not being involved in the assembly and disassembly of SGs, client proteins in SGs may play a crucial role in regulating signaling pathways<sup>23,25–27</sup>. Our data indicate that ATG proteins do not contribute to the driving force of SG assembly (Fig. 3d, e), suggesting that they act as client proteins within SGs. In yeast, the ATG1 complex has been shown to undergo liquid-liquid phase separation, leading to the formation of membraneless

condensates that organize the site of autophagosome formation<sup>55</sup>. In plants, whether ATG proteins possess similar phase-separation capabilities and how this might aid in their recruitment to SGs are intriguing questions that warrant further investigation. In this study, we found that the number of ATGs-labeled puncta significantly decreased in *ubp1abc* triple mutant compared to the WT plants after 1 h of HS (Fig. 3b, c). Given that the *ubp1abc* triple mutant showed an obvious defect in the formation of HS-induced SGs, as indicated by the core

**Fig. 5 | ATG8-labeled puncta co-localizes with NBRI-decorated particles during the HS recovery phase.** **a** The 5-day-old mCherry-ATG8f × UBPIc-GFP plants were subjected to HS treatment at 38 °C for 1 h, and then recovered at 22 °C for 3 h. The Meristem zone of indicated samples was observed using a confocal microscope. Scale bar = 10 μm. **b** The 5-day-old mCherry-ATG8f × NBRI-GFP plants were subjected to treatment at 22 °C (control) or 38 °C (HS) for 1 h, followed by heat-stressed plants recovered at 22 °C for 1 h and 3 h. The Meristem zone of indicated samples was observed using a confocal microscope. Scale bar = 10 μm. **c** Statistical analysis of the number of mCherry-ATG8f/NBRI-GFP colocalization foci signal in **(b)**. Data represent mean ± SD; *n* = 10. Ten different 50 × 50 μm<sup>2</sup> areas in the meristem zone were used for colocalization analysis. Statistical analysis was performed using a two-tailed unpaired Student's *t* test. **d** The 5-day-old mCherry-ATG8f × NBRI-GFP

plants were subjected to HS treatment at 38 °C for 1 h, followed by recovery at 22 °C for 9 h. The meristem zone of indicated samples was observed using a confocal microscope. Scale bar = 10 μm. **e** The 5-day-old mCherry-ATG8f × NBRI-GFP plants were subjected to treatment at 22 °C (control) or 38 °C (HS) for 1 h and then transferred to 1/2 MS liquid medium at 22 °C. After 6 h of recovery, 1 μM of Conc A was added to the medium, and the plants continued to recover for another 6 h. The maturation zone of the indicated samples was observed using a confocal microscope. Scale bar = 10 μm. **f** Statistical analysis of colocalizations between NBRI-GFP and mCherry-ATG8f inside vacuole in **(e)**. Data represent mean ± SD; *n* = 10. Ten different 50 × 50 μm<sup>2</sup> areas in the maturation zone were used for colocalization analysis. Statistical analysis was performed using a two-tailed unpaired Student's *t* test. Source data are provided as a Source Data file.

component mCherry-RBP47b (Supplementary Fig. 16e), the reduction in ATGs-labeled puncta in *ubp1abc* mutant might be attributed to the defect in SGs assembly. Therefore, despite observing an association between ATG proteins and components of SGs under HS conditions in vivo (Fig. 2), the precise scaffold components that are directly responsible for recruiting ATG proteins to SGs have yet to be identified.

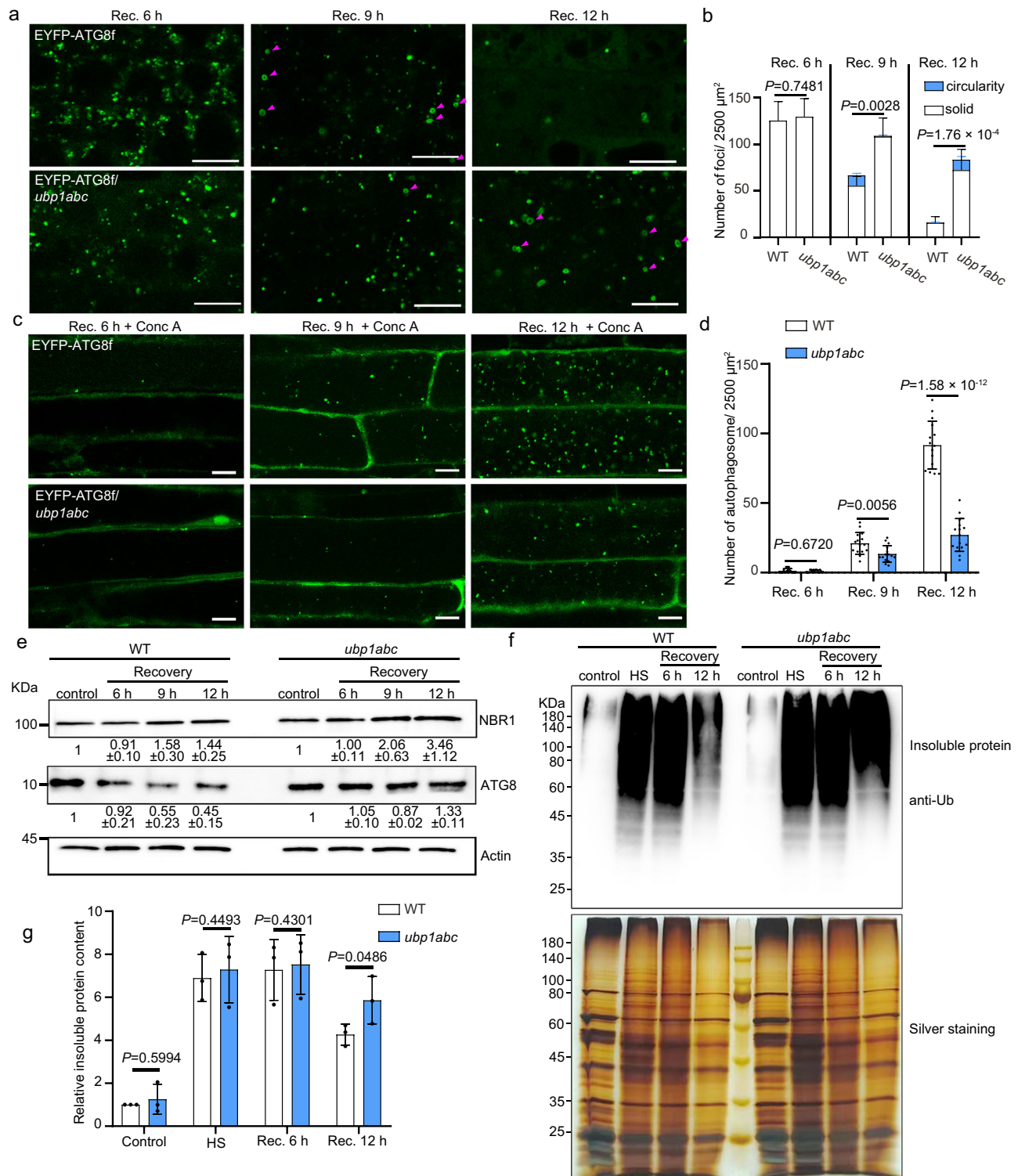
These ATG puncta were induced by HS, but not by osmotic stress, salt stress, drought stress, or oxidative stress (Supplementary Fig. 9b). This distinction suggests that HS-induced SGs play a unique role in regulating autophagic activity, unlike the SGs formed under other stress conditions. The initiation factor, components, mRNA types and functions of SGs vary significantly depending on the stressors. Different stressors activate distinct stress-related kinases to phosphorylate eIF2α, which causes translation suspension that is a prerequisite for SG assembly<sup>56</sup>. Consequently, the composition and the types of mRNAs of the different SGs are shaped by their initiating signals<sup>32</sup>. For instance, HS-induced SGs can bind the mRNA of heat shock proteins<sup>20</sup>, while hypoxia-induced SGs can bind hypoxia-responsive mRNAs<sup>17</sup>, illustrating that SGs perform functions based on their associated mRNA. Furthermore, heat-induced SGs can persist for approximately 6 h after the stress is relieved in the plant (Fig. 3d), while hypoxia-induced SGs can only be maintained for approximately 30 min<sup>17</sup>, further indicating substantial differences in the composition and regulatory mechanisms of various SG types. In addition, obvious differences in SGs induced by varying temperature intervals were also observed. Specifically, the number of SGs significantly increased, whereas their diameters seemed to show a notable reduction, as the temperature rose from 34 °C to 40 °C (Supplementary Fig. 4c–h). This suggests that SGs are sensitive to varying degrees of thermal stress, adjusting their response to ensure optimal energy efficiency and cellular regulation. Although the initiation conditions, composition, mRNA types, and function of SGs in mammals have been preliminarily identified, there is a considerable gap in our understanding of these aspects in plants. Future work involving mass spectrometry analysis of SG proteins and RNA sequencing will be essential to dissect the composition and function of different types of SGs. Such research will contribute to a more comprehensive understanding of the diverse roles that various SGs play in cellular processes in plants.

Previous studies have shown that SGs, which recruit key signaling molecules, can either sequester their signals<sup>23,26,27</sup> or protect them from thermal denaturation<sup>25</sup>. Here, we demonstrated that autophagosome formation was temporally inhibited during the HS phase, while was boosted during the post-HS recovery phase (Fig. 4a and Supplementary Fig. 14), indicating that SGs are involved in the sequestration of the ATG proteins. Nonetheless, further investigation is required to determine if ATG protein levels in *ubp1abc* mutant decrease after HS compared to wild type. This will help confirm whether SGs serve as temporary reservoirs, similar to a repository of mRNA, thereby safeguarding these ATG proteins from thermal denaturation and ensuring their rapid availability after the stress is

alleviated. A recent study has proposed that SGs can serve as platforms for activating the SnRK1 kinase activity upon HS<sup>28</sup>. Our findings showed that the lipidation of ATG8 was promptly suppressed during HS phase, but upon the alleviation of heat stress, the PE modification of ATG8 was rapidly enhanced (Supplementary Fig. 14). However, in the *ubp1abc* mutant with deficient in SGs assembly, the ATG8 lipidation was not sufficiently activated compared to that in WT plants (Supplementary Fig. 14). These observations motivated us to hypothesize that SGs may serve as docking platform to expedite the ATG8-PE modification and trigger autophagy during the recovery phase. Exploring this hypothesis in future work will enhance our understanding of the biological significance of ATG protein translocation to SGs in plants.

During the HS recovery phase, NBRI-decorated particles gradually recruit ATG8, leading to the appearance of a cup-shaped structure that may facilitate autophagosome formation (Figs. 4 and 5). However, the mechanism by which NBRI-decorated membraneless condensates transform into the cup-shaped structure and subsequently the ring autophagosome structure remains unknown in plants. In mammals, upon the addition of the K63 polyubiquitinated chain, p62/SQSTM1 undergoes liquid-liquid phase separation, resulting in the formation of membraneless condensates that serve as anchors to recruit autophagy components, thereby facilitating autophagosome formation<sup>57,58</sup>. Whether a similar mechanism exists in plants is yet to be determined. NBRI has been identified as an autophagy receptor for K63-ubiquitinated protein in plants, and shares features of both NBRI and mammalian p62<sup>9</sup>. Furthermore, NBRI is known to contain two typical IDRs (Internally disordered region, 168aa-230aa and 503aa-575aa), but it remains unclear whether these IDRs confer the phase-separation ability of NBRI. Consequently, it is plausible to hypothesize that a combination of NBRI and ATG8 after HS may be favorable for the initiation of autophagy that facilitates the clearance of ubiquitinated cargoes.

Previous studies have indicated the involvement of the autophagy pathway in degrading components within persistent SGs caused by prolonged stress or disease mutations in mammals<sup>37,38,59,60</sup>. Nevertheless, the disassembly of SGs transiently induced by treatments such as HS or sodium arsenite is not influenced by the autophagy pathway, but is primarily regulated by K63 ubiquitination modification of G3BP1/2<sup>38,61,62</sup>. Autophagy-mediated clearance of SGs can result in the complete degradation of proteins and RNA within the SGs. In contrast to SGs clearance, SGs disassembly only requires the degradation of certain scaffold proteins or the weakening of internal protein-protein interactions, allowing the internal proteins and RNA to be recycled<sup>61</sup>. Similar to the mechanism in mammals<sup>38</sup>, SGs disassembly was not affected in the plant autophagy-deficient mutants (Fig. 3e). Previous studies have demonstrated that AAA ATPase p97/CDC48/VCP can form hexamers to separate ubiquitinated substrates from stable protein components, membranes, and chromatin, facilitating their entry into proteasomal or autophagic degradation<sup>63</sup>. VCP is recruited to SGs during HS and phosphorylated by ULK1/2, playing a crucial role in SGs disassembly, but this process is autophagy-independent<sup>38,61,62</sup>. Future



studies are needed to identify the factors required for the disassembly of HS-induced SGs and elucidate their possible roles in autophagy activation after HS.

## Methods

### Plant materials and growth conditions

In this study, all plants were *Arabidopsis thaliana* Col-0 background. All seeds were sterilized and stored at 4 °C for 2–3 days in the dark. The seeds were grown on 1/2 MS agar medium containing 1% (v/v) sucrose at 22 °C under LD (16 h light/8 h dark) conditions. The *ubp1a-1* (GK-625F11-022320) and *ubp1b-1* (GK-262E01-014951) mutants were

obtained from the Arabidopsis Biological Resource Center (ABRC). The knockout of the *UBP1c* mutant (*ubp1c-cas9*) was generated using an egg-specific promoter-driven CRISPR-Cas9-edited system, followed by segregation of the Cas9 transgene by backcrossing to the WT<sup>64</sup>. As a result, a 427 bp region of the *UBP1c* gene region was deleted (Supplementary Fig. 16b, c), which is a null mutant (Supplementary Fig. 16d). The triple loss-of-function mutant *ubp1abc* was generated by pollen crossing *ubp1a-1*, *ubp1b-1*, and *ubp1c-cas9*, which was verified by genotyping (Supplementary Fig. 16d). The *pUBQ10::ATG5-GFP*, *pUBQ10::ATG9-GFP*, *pUBQ10::EYFP-ATG8f*, *pUBQ10::ATG18a-GFP*, *pUBQ10::mCherry-ATG8f* × *pUBQ10::NBR1-GFP*, *pUBQ10::mCherry-ATG8f* ×

**Fig. 6 | Autophagy activation is slowed in *ubp1abc* mutant during the recovery from HS.** **a** The 5-day-old EYFP-ATG8f/WT and EYFP-ATG8f/*ubp1abc* plants were subjected to HS treatment at 38 °C for 1 h, and then recovered at 22 °C for 6 h, 9 h, and 12 h. The maturation zone of indicated samples was observed using a confocal microscope. Scale bar = 10 μm. The magenta triangle represents circular structures. **b** Statistical analysis of the number of punctate signals in (a). Data represent mean ± SD; *n* = 5. Statistical analysis was performed using a two-tailed unpaired Student's *t* test. **c** The 5-day-old EYFP-ATG8f/WT and EYFP-ATG8f/*ubp1abc* plants were subjected to HS treatment at 38 °C HS for 1 h, and then recovered in 1/2 MS liquid medium supplemented with 1 μM Conc A for 6 h, 9 h, and 12 h at 22 °C. The maturation zone of the roots from the indicated samples was observed using a confocal microscope. Scale bar = 10 μm. **d** Statistical analysis of the number of autophagosomes in (c). Data represent mean ± SD; *n* = 15. Statistical analysis was performed using a two-tailed unpaired Student's *t* test. **e** The 5-day-old WT and

*ubp1abc* plants were subjected to treatment at 22 °C (control) or 38 °C (HS) for 1 h and then heat-stressed plants recovered at 22 °C for 6 h, 9 h, and 12 h. Total proteins were extracted to detect using Anti-NBR1 (Agrisera; Cat# AS14 2805 A; 1:3000) and Anti-ATG8 (Agrisera; Cat# AS14 2769; 1:3000), with Anti-actin (Sangon Biotech; Cat# D110007; 1:5000) as the internal control. The value represents the relative protein content, defining the control group as 1. Data represent mean ± SEM; *n* = 3. **f** The 5-day-old WT and *ubp1abc* plants were subjected to treatment at 22 °C (control) or 38 °C (HS) for 1 h and then heat-stressed plants recovered at 22 °C for 6 h and 12 h. The same amount of insoluble protein was separated by SDS-PAGE and then stained with silver stain, which was used as a loading control. **g** Statistical analysis of the insoluble protein content in (f). Data represent the mean ± SD; *n* = 3. Statistical analyses were performed using a two-tailed paired Student's *t* test. Source data are provided as a Source Data file.

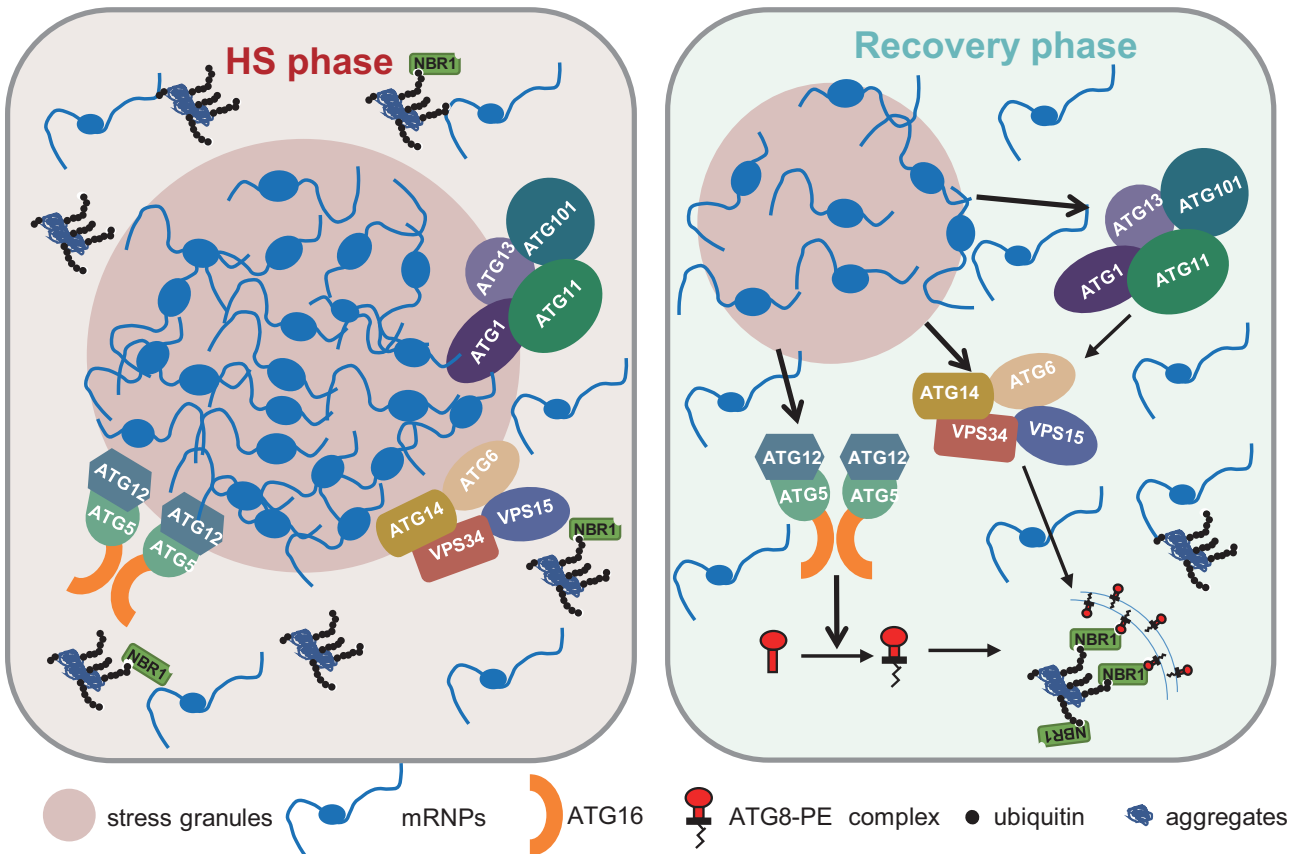


**Fig. 7 | Schematic model of the role of SGs in sequestering ATG proteins upon HS.** During the HS phase, the ATG1/ATG13 complex, PI3K complex, and ATG5-ATG12 complex are recruited to SGs, resulting in the inhibition of autophagy.

During the HS recovery phase, ATG proteins are released as SGs disassemble, thereby promoting autophagy to remove ubiquitinated proteins.

*pUBQ10::GFP-SYP32*, and *atg5-1* mutants have been described previously<sup>29,31,40,65</sup>. The *pUBQ10::ATG1a-GFP*, *pUBQ10::ATG13a-GFP*, *pUBQ10::ATG6-GFP*, *pUBQ10::GFP-VPS34*, *pUBQ10::ATG3-GFP*, *pUBQ10::ATG7-GFP*, *pUBQ10::UBP1c-mCherry*, *pUBQ10::UBP1c-GFP*, *pUBQ10::ATG13a-GFP/ubp1abc*, *pUBQ10::ATG6-GFP/ubp1abc*, *pUBQ10::ATG5-GFP/ubp1abc*, *pUBQ10::EYFP-ATG8f/ubp1abc*, *pUBQ10::mCherry-RBP47b*, *pUBQ10::mCherry-RBP47b/ubp1abc* plants were generated using the floral dip method with *Agrobacterium tumefaciens* GV3101<sup>66</sup>. T3 homozygous lines were selected for further analysis. The *pUBQ10::ATG13a-GFP×pUBQ10::UBP1c-mCherry*, *pUBQ10::ATG6-GFP×pUBQ10::UBP1c-mCherry*, *pUBQ10::ATG5-GFP×pUBQ10::UBP1c-mCherry*, *pUBQ10::ATG9-GFP×pUBQ10::UBP1c-mCherry*, *pUBQ10::UBP1c-GFP×pUBQ10::mCherry-ATG8f*, *pUBQ10::ATG13a-GFP×mRFP-Rha1*, *pUBQ10::ATG6-GFP×mRFP-Rha1*, *pUBQ10::ATG5-GFP×mRFP-Rha1*, *pUBQ10::AT*

*G13a-GFP×Mito-mRFP*, *pUBQ10::ATG6-GFP×Mito-mRFP*, *pUBQ10::ATG5-GFP×Mito-mRFP*, *pUBQ10::ATG13a-GFP×mRFP-SYP32*, *pUBQ10::ATG6-GFP×mRFP-SYP32*, *pUBQ10::ATG5-GFP×mRFP-SYP32*, *pUBQ10::ATG13a-GFP×VHAa1-mRFP*, *pUBQ10::ATG6-GFP×VHAa1-mRFP*, *pUBQ10::ATG5-GFP×VHAa1-mRFP*, *pUBQ10::UBP1c-GFP/atg5-1* plants were generated by pollen crossing. The marker lines *VHAa1-mRFP*, *mRFP-SYP32*, *Mito-mRFP*, and *mRFP-Rha1* have been described previously<sup>67–69</sup>. The primers are listed in Supplementary Table 1.

### Stress treatment

The plants were grown on 1/2 MS agar medium containing 1% (v/v) sucrose at 22 °C under LD conditions for 5 days. For the HS treatment, 20–30 plants were transferred to 12-well culture dishes containing 1/2 MS liquid medium and placed in a water bath at 22 °C (control) or 38 °C

(HS) for 1 h on the bench. In the subsequent HS recovery phase, the plants were transferred to 1/2 MS solid plates or 1/2 MS liquid medium supplemented with 1  $\mu$ M Conc A for observation of autophagosomes and placed in a plant growth chamber at 22 °C. For the HS + CHX treatment, 15–20 plants were transferred to 12-well culture dishes containing 1/2 MS liquid medium supplemented with 50  $\mu$ M CHX and placed in a plant growth chamber at 22 °C for a 30 min pretreatment. Subsequently, the dishes were transferred to a water bath at 38 °C for 1 h. For osmotic, salt, drought, and oxidative stress, 20–30 plants were transferred to 12-well culture dishes containing 1/2 MS liquid medium with 300 mM mannitol for 6 h, 300 mM NaCl for 6 h, 20% (w/v) PEG4000 for 6 h or 0.5 mM Arsenite for 1 h and then placed in a plant growth chamber at 22 °C, respectively. Subsequently, the indicated samples were observed using confocal microscopy or subjected to quick freezing in liquid nitrogen for the isolation of SGs and insoluble proteins, or Co-IP assay.

### Co-immunoprecipitation (Co-IP)

For Co-IP experiments, different combinations (Fig. 2b–d) of vectors were transiently transformed into protoplasts of Arabidopsis mediated by PEG4000 according to our previously established method<sup>70</sup>. After incubation in darkness for 12–14 h, the protoplast cells were transferred to a metal bath at 22 °C (control) or 38 °C (HS) for 1 h, followed by a collection for total protein extraction for Co-IP. The proteins were isolated using IP buffer (50 mM Tris pH 8.0, 150 mM NaCl, 1 mM MgCl<sub>2</sub>, 0.2% (v/v) Triton X-100, and 1 $\times$  Roche protease inhibitor cocktail). After centrifugation at 600  $\times$  g, the cell debris was removed, and 20  $\mu$ L of GFP-Trap magnetic beads (SM038001, Smart-Lifesciences) were washed twice with IP buffer. The beads were then resuspended in the mixed liquors and incubated for 2 h at 4 °C with gentle rotation. Subsequently, the Mag-Beads were washed four times for 3 min with an IP buffer. The protein was eluted using 2  $\times$  SDS protein extraction buffer [100 mM Tris (pH 6.8), 4% (v/v) SDS, 20% (v/v) glycerol, 10% (v/v)  $\beta$ -mercaptoethanol, and 0.2 mg·ml<sup>-1</sup> Bromophenol Blue] at 95 °C for 5 min. The proteins were loaded onto 10% SDS-PAGE gels for immunoblot analysis using anti-GFP (Transgene; Cat# HT801-01; 1:5000) and anti-FLAG (Transgene; Cat# HT201-01; 1:5000) antibodies.

### Bimolecular fluorescence complementation (BiFC) analysis, transient expression in tobacco leaves

The BiFC assay was performed according to a previously established method<sup>71,72</sup>. The full-length CDS of *UBP1a* and *GUS* was cloned into the *pCAMBIA1300* binary vector to fuse in-frame with cYFP (155aa–239aa) driven by the *UBQ10* promoter. The full-length CDS of *ATG1a*, *ATG13a*, *ATG6*, *VPS34*, *ATG5*, *ATG3*, and *RBP47b* were cloned into the *pCAMBIA1300* binary vector to fuse in-frame with nYFP (1aa–173aa) driven by the *UBQ10* promoter. Each vector was individually transformed into *Agrobacterium tumefaciens* strain GV3101. *Agrobacterium tumefaciens* growing to the logarithmic phase was resuspended in injection buffer (10 mM MgCl<sub>2</sub>, 10 mM MES [pH 5.6], 150  $\mu$ M acetosyringone). Subsequently, the suspension was adjusted to OD<sub>600</sub> = 1.0 and incubated for at least 3 h in the dark at room temperature. For transient expression in tobacco leaves, 4-week-old tobacco (*Nicotiana benthamiana*) plants were infiltrated with *Agrobacterium* after mixing in equal proportions, as indicated. After a 48-h period of expression, the fluorescence signal was detected by confocal microscopy with and without HS treatment at 38 °C.

### Transmission electron microscopy (TEM) analysis

The 5-day-old plants were subjected to HS at 38 °C for 1 h, followed by a recovery period of 3 h or 9 h at 22 °C. At the indicated times, the root tips were collected and frozen in liquid nitrogen using a high-pressure freezing machine (HPM100, Leica). The samples were subsequently substituted with anhydrous acetone containing 0.25% glutaraldehyde and 0.1% uranyl acetate and frozen at –80 °C for 24 h.

After slowly warming the samples to –20 °C, they were rinsed with pre-chilled acetone and embedded in HM20 resin. Thin sections (100 nm) were prepared and incubated with a GFP primary antibody (Abcam; Cat# ab290; 1:1000) for 4 h at room temperature. After conjugation with gold particle-coupled secondary antibodies at a dilution of 1/50 (goat anti-rabbit IgG), 10 nm (Electron Microscopy Sciences), the grids were post-stained and examined using a Hitachi 7400 transmission electron microscope (Hitachi High Technologies) operated at 80 KV.

### Separation of SGs-enriched fraction by differential centrifugation

The method for the separation of SGs was adapted from previous studies with the objective of facilitating the collection of precipitation and supernatant from cell lysis<sup>22</sup>. Different combinations (Fig. 2h and Supplementary Fig. 6) of vectors were transiently transformed into protoplasts of Arabidopsis mediated by PEG4000, according to our previously established method<sup>70</sup>. After incubation in darkness for 12–14 h, the protoplast cells (approximately 5  $\times$  10<sup>5</sup> cells) were transferred to a water bath at 22 °C (control) or 38 °C (HS) for 1 h, followed by centrifugation collection and liquid nitrogen quick freezing. Each sample was added to 500  $\mu$ L of pre-cooled protein extraction buffer (50 mM Tris (pH 8.0), 150 mM NaCl, 1 mM MgCl<sub>2</sub>, 0.2% (v/v) Triton X-100, and 1 $\times$  Roche protease inhibitor cocktail), followed by vortexing at room temperature for 3 min and incubation on ice for 5 min for complete lysis. After centrifugation at 600  $\times$  g at 4 °C twice for 3 min to remove cell debris, 50  $\mu$ L of the mixed liquor was collected as total protein (T). Subsequently, 400  $\mu$ L of the mixed liquor was further centrifuged at 12,000  $\times$  g at 4 °C for 5 min, and 50  $\mu$ L supernatant was collected as the supernatant protein (S). Next, the pellet was resuspended in protein extraction buffer for washing, followed by centrifugation 12,000  $\times$  g at 4 °C for 1 min, repeated three times. Finally, the pellet protein (P) was resuspended in 400  $\mu$ L of protein extraction buffer. An equal amount of the sample was added to 2  $\times$  SDS protein extraction buffer and then denatured by heating at 95 °C for 5 min. Equal proportion of denatured samples were separated by 10% SDS-PAGE detected by western blotting using Anti-FLAG (Transgene; Cat# HT201-01; 1:5000) and Anti-GFP (Transgene; Cat# HT801-01; 1:5000) or Anti-mCherry (HUABIO; Cat# HA601186; 1:5000). For visual observation, the precipitate was resuspended in 50  $\mu$ L protein extraction buffer, followed by 5  $\mu$ L suspension sucked into the confocal dish for confocal observation.

### Microscopy analysis and image processing

Fluorescence images were obtained using an LSM880 confocal microscope with a  $\times$ 63/1.4 oil objective under 514 nm excitation and detection with a 520–560 nm filter for YFP, 488 nm excitation and detection with a 500–550 nm filter for GFP, and 561 nm excitation and detection with a 575–650 nm filter for mCherry. Image analysis and processing were performed using ZEISS ZEN software v.2.5 and Adobe Photoshop (version 23.0.0).

The Trainable Weka Segmentation plugin in ImageJ software was used for statistical analysis of punctate signals according to previous research<sup>51,73</sup>. First, a suitable confocal image for each experiment was selected, and then the punctate signals were manually outlined in the Trainable Weka Segmentation plugin and set as class 1, while the background signals were also outlined and set as class 2. The classifier was then trained on this image. Subsequently, the process is repeated to outline punctate or background signals that the machine is unable to recognize. The machine was trained multiple times, and the classifier parameter was saved for application to other images. After the image to be analyzed has been processed by the classifier, the watershed module is used to segment the overlapping punctate signals. The Analyze Particles module was used for counting. For the statistical analysis of co-localized point signals, the same plugin was used with slight variations. First, a merged image must be split into

different channels. Automatic labeling of punctate signals in each channel was then performed. Subsequently, the ROI Manager module was used to merge the two different channels, followed by counting the overlapping and non-overlapping areas. At least ten images of different areas from five individual plants were used for colocalization analysis.

For fluorescence colocalization analysis, the Coloc 2 plugin in the ImageJ software was used for the Pearson correlation coefficient calculation. First, the Split channels function in ImageJ was used to split the merged fluorescence image, and then the Coloc 2 plugin was used to calculate the Pearson coefficients of the green and red channels using the default parameters of the software. At least three images from different regions were used for colocalization analysis. The values are marked in the indicated images.

### Insoluble protein separation for ubiquitination detection

After HS and HS recovery, 0.3 g of plant samples were ground into powder in liquid nitrogen to extract total protein using 1 mL of pre-cooled protein extraction buffer [50 mM Tris (pH 7.5), 150 mM NaCl, 1 mM MgCl<sub>2</sub>, 0.1% Triton X-100, 1× Roche protease inhibitor cocktail, and 10 mM N-ethylmaleimide], followed by fully mix them using a grinding rod. Cell debris was removed by centrifugation at 600 × g twice at 4 °C. Subsequently, the lysate was centrifuged at 18,000 × g at 4 °C for 10 min. Next, the insoluble protein was resuspended in 200 μL of protein extraction buffer, followed by centrifugation at 18,000 × g at 4 °C for 5 min, which was repeated three times. Finally, the insoluble protein was resuspended in 100 μL 2 × SDS protein extraction buffer. Equal proportions of denatured samples were separated by 12% SDS-PAGE and detected by western blotting using Ubiquitin1I antibodies (Agriseria; Cat# AS08307A; 1:5000). The same amount of insoluble protein was separated by SDS-PAGE and then stained with silver stain, which was used as a loading control.

### Statistics and Reproducibility

Statistical differences were calculated using one-way analysis of variance (ANOVA) or two-tailed unpaired and paired Student's *t* test using GraphPad Prism software (version 8.0.1). The statistical analysis for each experiment is described in the figure legends. The *P* value < 0.05 was considered to indicate statistical significance. For representative data such as Figs. 1a, d; 2b–d, f, g; 3a, f; 4c; 5a, d and Supplementary Figs. 1a, b; 4a, b; 5a–c; 6a–d; 7a, b; 9a, b; 10a, b; 11a, b; 12a, b at least three biological replications were shown, each time at least five different plants were observed with the same result.

### Reporting summary

Further information on research design is available in the Nature Portfolio Reporting Summary linked to this article.

### Data availability

The main data supporting the findings of this study are available within the article and its Supplementary Figures. The source data underlying Figs. 1–6, Supplementary Figs. 4, 8, 13, 14, and 16 are provided as a Source Data file. Source data are provided with this paper.

### References

- Bokszczanin, K. L. Solanaceae Pollen Thermotolerance Initial Training Network C, Fragkostefanakis S. Perspectives on deciphering mechanisms underlying plant heat stress response and thermotolerance. *Front. Plant Sci.* **4**, 315 (2013).
- McClung, C. R. & Davis, S. J. Ambient thermometers in plants: from physiological outputs towards mechanisms of thermal sensing. *Curr. Biol.* **20**, R1086–R1092 (2010).
- Kan, Y., Mu, X. R., Gao, J., Lin, H. X. & Lin, Y. The molecular basis of heat stress responses in plants. *Mol. Plant* **16**, 1612–1634 (2023).
- Rossi, S. & Huang, B. Regulatory roles of morphactin on suppressing chlorophyll degradation under heat stress in creeping bentgrass. *Grass Res.* **3**, 11 (2023).
- Zhou, J. et al. NBR1-mediated selective autophagy targets insoluble ubiquitinated protein aggregates in plant stress responses. *PLoS Genet.* **9**, e1003196 (2013).
- Sedaghatmehr, M. et al. A regulatory role of autophagy for resetting the memory of heat stress in plants. *Plant Cell Environ.* **42**, 1054–1064 (2019).
- Zhou, J., Wang, J., Yu, J. Q. & Chen, Z. Role and regulation of autophagy in heat stress responses of tomato plants. *Front. Plant Sci.* **5**, 174 (2014).
- Svenning, S., Lamark, T., Krause, K. & Johansen, T. Plant NBR1 is a selective autophagy substrate and a functional hybrid of the mammalian autophagic adapters NBR1 and p62/SQSTM1. *Autophagy* **7**, 993–1010 (2011).
- Zhou, J. et al. E3 ubiquitin ligase CHIP and NBR1-mediated selective autophagy protect additively against proteotoxicity in plant stress responses. *PLoS Genet.* **10**, e1004116 (2014).
- Protter, D. S. W. & Parker, R. Principles and properties of stress granules. *Trends Cell Biol.* **26**, 668–679 (2016).
- Maruri-Lopez, I., Figueroa, N. E., Hernandez-Sanchez, I. E. & Chodasiewicz, M. Plant stress granules: trends and beyond. *Front. Plant Sci.* **12**, 722643 (2021).
- Wang, H. et al. A double-stranded RNA binding protein enhances drought resistance via protein phase separation in rice. *Nat. Commun.* **15**, 2514 (2024).
- Nguyen, C. C. et al. Oligouridylate binding protein 1b plays an integral role in plant heat stress tolerance. *Front. Plant Sci.* **7**, 853 (2016).
- Gutierrez-Beltran, E., Moschou, P. N., Smertenko, A. P. & Bozhkov, P. V. Tudor staphylococcal nuclease links formation of stress granules and processing bodies with mRNA catabolism in Arabidopsis. *Plant Cell* **27**, 926–943 (2015).
- Yan, C., Yan, Z., Wang, Y., Yan, X. & Han, Y. Tudor-SN, a component of stress granules, regulates growth under salt stress by modulating GA20ox3 mRNA levels in Arabidopsis. *J. Exp. Bot.* **65**, 5933–5944 (2014).
- Weber, C., Nover, L. & Fauth, M. Plant stress granules and mRNA processing bodies are distinct from heat stress granules. *Plant J.* **56**, 517–530 (2008).
- Sorenson, R. & Bailey-Serres, J. Selective mRNA sequestration by OLIGOURIDYLATE-BINDING PROTEIN 1 contributes to translational control during hypoxia in Arabidopsis. *Proc. Natl Acad. Sci. USA* **111**, 2373–2378 (2014).
- Wu, X. et al. N6-methyladenosine-mediated feedback regulation of abscisic acid perception via phase-separated ECT8 condensates in Arabidopsis. *Nat. Plants* **10**, 469–482 (2024).
- Xie, Z. et al. Phenolic acid-induced phase separation and translation inhibition mediate plant interspecific competition. *Nat. Plants* **9**, 1481–1499 (2023).
- Tong, J. et al. ALBA proteins confer thermotolerance through stabilizing HSF messenger RNAs in cytoplasmic granules. *Nat. Plants* **8**, 778–791 (2022).
- Zhu, S. et al. Liquid-liquid phase separation of RBGD2/4 is required for heat stress resistance in Arabidopsis. *Dev. Cell* **57**, 583–597 (2022).
- Kosmacz, M. et al. Protein and metabolite composition of Arabidopsis stress granules. *N. Phytol.* **222**, 1420–1433 (2019).
- Takahara, T. & Maeda, T. Transient sequestration of TORC1 into stress granules during heat stress. *Mol. Cell* **47**, 242–252 (2012).
- Thedieck, K. et al. Inhibition of mTORC1 by astrin and stress granules prevents apoptosis in cancer cells. *Cell* **154**, 859–874 (2013).

25. Qin, W. et al. Dynamic mapping of proteome trafficking within and between living cells by TransitID. *Cell* **186**, 3307–3324.e3330 (2023).
26. Kim, W. J., Back, S. H., Kim, V., Ryu, I. & Jang, S. K. Sequestration of TRAF2 into stress granules interrupts tumor necrosis factor signaling under stress conditions. *Mol. Cell. Biol.* **25**, 2450–2462 (2005).
27. Arimoto, K., Fukuda, H., Imajoh-Ohmi, S., Saito, H. & Takekawa, M. Formation of stress granules inhibits apoptosis by suppressing stress-responsive MAPK pathways. *Nat. Cell Biol.* **10**, 1324–1332 (2008).
28. Gutierrez-Beltran, E. et al. Tudor staphylococcal nuclease is a docking platform for stress granule components and is essential for SnRK1 activation in Arabidopsis. *EMBO J.* **40**, e105043 (2021).
29. Zhou, J. et al. A non-canonical role of ATG8 in Golgi recovery from heat stress in plants. *Nat. Plants* **9**, 749–765 (2023).
30. Hamada, T. et al. Stress granule formation is induced by a threshold temperature rather than a temperature difference in Arabidopsis. *J. Cell Sci.* **131**, jcs216051 (2018).
31. Zhuang, X. et al. ATG9 regulates autophagosome progression from the endoplasmic reticulum in Arabidopsis. *Proc. Natl Acad. Sci. USA* **114**, E426–E435 (2017).
32. Markmiller, S. et al. Context-dependent and disease-specific diversity in protein interactions within stress granules. *Cell* **172**, 590–604.e513 (2018).
33. Sanders, D. W. et al. Competing protein-RNA interaction networks control multiphase intracellular organization. *Cell* **181**, 306–324.e328 (2020).
34. Wilczynska, A., Aigueperse, C., Kress, M., Dautry, F. & Weil, D. The translational regulator CPEB1 provides a link between dcp1 bodies and stress granules. *J. Cell Sci.* **118**, 981–992 (2005).
35. Gilks, N. et al. Stress granule assembly is mediated by prion-like aggregation of TIA-1. *Mol. Biol. Cell* **15**, 5383–5398 (2004).
36. Yang, P. et al. G3BP1 is a tunable switch that triggers phase separation to assemble stress granules. *Cell* **181**, 325–345.e328 (2020).
37. Buchan, J. R., Kolaitis, R. M., Taylor, J. P. & Parker, R. Eukaryotic stress granules are cleared by autophagy and Cdc48/VCP function. *Cell* **153**, 1461–1474 (2013).
38. Wang, B. et al. ULK1 and ULK2 regulate stress granule disassembly through phosphorylation and activation of VCP/p97. *Mol. Cell* **74**, 742–757.e748 (2019).
39. Jung, H. et al. Arabidopsis cargo receptor NBR1 mediates selective autophagy of defective proteins. *J. Exp. Bot.* **71**, 73–89 (2020).
40. Thompson, A. R., Doelling, J. H., Suttangkakul, A. & Vierstra, R. D. Autophagic nutrient recycling in Arabidopsis directed by the ATG8 and ATG12 conjugation pathways. *Plant Physiol.* **138**, 2097–2110 (2005).
41. Yoshimoto, K. et al. Processing of ATG8s, ubiquitin-like proteins, and their deconjugation by ATG4s are essential for plant autophagy. *Plant Cell* **16**, 2967–2983 (2004).
42. Qi, H. et al. Studying plant autophagy: challenges and recommended methodologies. *Adv. Biotechnol.* **1**, 2 (2023).
43. Li, F. & Vierstra, R. D. Autophagy: a multifaceted intracellular system for bulk and selective recycling. *Trends Plant Sci.* **17**, 526–537 (2012).
44. Marshall, R. S. & Vierstra, R. D. Autophagy: the master of bulk and selective recycling. *Annu Rev. Plant Biol.* **69**, 173–208 (2018).
45. Yang, C. et al. HY5-HDA9 module transcriptionally regulates plant autophagy in response to light-to-dark conversion and nitrogen starvation. *Mol. Plant* **13**, 515–531 (2020).
46. Li, X. et al. Arabidopsis flowering integrator SOC1 transcriptionally regulates autophagy in response to long-term carbon starvation. *J. Exp. Bot.* **73**, 6589–6599 (2022).
47. Li, B. et al. Ufmylation reconciles salt stress-induced unfolded protein responses via ER-phagy in Arabidopsis. *Proc. Natl Acad. Sci. USA* **120**, e2208351120 (2023).
48. Thirumalaikumar, V. P. et al. Selective autophagy regulates heat stress memory in Arabidopsis by NBR1-mediated targeting of HSP90.1 and ROF1. *Autophagy* **17**, 2184–2199 (2021).
49. Li, F., Chung, T. & Vierstra, R. D. AUTOPHAGY-RELATED11 plays a critical role in general autophagy- and senescence-induced mitophagy in Arabidopsis. *Plant Cell* **26**, 788–807 (2014).
50. Suttangkakul, A., Li, F., Chung, T. & Vierstra, R. D. The ATG1/ATG13 protein kinase complex is both a regulator and a target of autophagic recycling in Arabidopsis. *Plant Cell* **23**, 3761–3779 (2011).
51. Yang, C. et al. A positive feedback regulation of SnRK1 signaling by autophagy in plants. *Mol. Plant* **16**, 1192–1211 (2023).
52. Banani, S. F. et al. Compositional control of phase-separated cellular bodies. *Cell* **166**, 651–663 (2016).
53. Schmit, J. D., Feric, M. & Dundr, M. How hierarchical interactions make membraneless organelles tick like clockwork. *Trends Biochem. Sci.* **46**, 525–534 (2021).
54. Espinosa, J. R. et al. Liquid network connectivity regulates the stability and composition of biomolecular condensates with many components. *Proc. Natl Acad. Sci. USA* **117**, 13238–13247 (2020).
55. Fujioka, Y. et al. Phase separation organizes the site of autophagosome formation. *Nature* **578**, 301–305 (2020).
56. Kedersha, N., Ivanov, P. & Anderson, P. Stress granules and cell signaling: more than just a passing phase? *Trends Biochem. Sci.* **38**, 494–506 (2013).
57. Feng, X. et al. Local membrane source gathering by p62 body drives autophagosome formation. *Nat. Commun.* **14**, 7338 (2023).
58. Sun, D., Wu, R., Zheng, J., Li, P. & Yu, L. Polyubiquitin chain-induced p62 phase separation drives autophagic cargo segregation. *Cell Res.* **28**, 405–415 (2018).
59. Yang, C. et al. Stress granule homeostasis is modulated by TRIM21-mediated ubiquitination of G3BP1 and autophagy-dependent elimination of stress granules. *Autophagy* **19**, 1934–1951 (2023).
60. Chitiprolu, M. et al. A complex of C9ORF72 and p62 uses arginine methylation to eliminate stress granules by autophagy. *Nat. Commun.* **9**, 2794 (2018).
61. Gwon, Y. et al. Ubiquitination of G3BP1 mediates stress granule disassembly in a context-specific manner. *Science* **372**, eabf6548 (2021).
62. Turakhiya, A. et al. ZFAND1 recruits p97 and the 26S proteasome to promote the clearance of arsenite-induced stress granules. *Mol. Cell* **70**, 906–919.e907 (2018).
63. Meyer, H., Bug, M. & Bremer, S. Emerging functions of the VCP/p97 AAA-ATPase in the ubiquitin system. *Nat. Cell Biol.* **14**, 117–123 (2012).
64. Wang, Z. P. et al. Egg cell-specific promoter-controlled CRISPR/Cas9 efficiently generates homozygous mutants for multiple target genes in Arabidopsis in a single generation. *Genome Biol.* **16**, 144 (2015).
65. Huang, L., Wen, X., Jin, L., Han, H. & Guo, H. HOOKLESS1 acetylates AUTOPHAGY-RELATED PROTEIN18a to promote autophagy during nutrient starvation in Arabidopsis. *Plant Cell* **36**, 136–157 (2023).
66. Clough, S. J. & Bent, A. F. Floral dip: a simplified method for Agrobacterium-mediated transformation of Arabidopsis thaliana. *Plant J.* **16**, 735–743 (1998).
67. Geldner, N. et al. Rapid, combinatorial analysis of membrane compartments in intact plants with a multicolor marker set. *Plant J.* **59**, 169–178 (2009).
68. Gao, C. et al. A unique plant ESCRT component, FREE1, regulates multivesicular body protein sorting and plant growth. *Curr. Biol.* **24**, 2556–2563 (2014).
69. El Zawily, A. M. et al. FRIENDLY regulates mitochondrial distribution, fusion, and quality control in Arabidopsis. *Plant Physiol.* **166**, 808–828 (2014).
70. Li, H. et al. The plant ESCRT component FREE1 shuttles to the nucleus to attenuate abscisic acid signalling. *Nat. Plants* **5**, 512–524 (2019).

71. Yang, C. et al. ABI5-FLZ13 module transcriptionally represses growth-related genes to delay seed germination in response to ABA. *Plant Commun.* **4**, 100636 (2023).
72. Li, X. et al. FLZ13 interacts with FLC and ABI5 to negatively regulate flowering time in Arabidopsis. *N. Phytol.* **241**, 1334–1347 (2024).
73. Arganda-Carreras, I. et al. Trainable Weka Segmentation: a machine learning tool for microscopy pixel classification. *Bioinformatics* **33**, 2424–2426 (2017).

## Acknowledgements

We thank Prof. Hongwei Guo (Southern University of Science and Technology) for kindly providing us with the ATG18a-GFP transgenic plants. This work was supported by grants from the National Natural Science Foundation of China (32270291, 32061160467), the Open Competition Program of Top Ten Critical Priorities of Agricultural Science and Technology Innovation for the 14th Five-Year Plan of Guangdong Province (2022SDZG05) and the Guangdong Province Rural Revitalization Strategy Special Funding for Seed Industry Vitalization to C.G., China Postdoctoral Science Foundation (2023M741234) to L.F., China Postdoctoral Science Foundation (2022M721220) to C.L., the National Science Foundation of China (31600288) and the Basic Research Program of Guangzhou (grant no. 202201010508) to J.Z., the National Natural Science Foundation of China (32000365, 32370329) and Guangdong Province grant (2021A1515010913) to H.L., and the National Natural Science Foundation of China (32222087), the Research Grants Council of Hong Kong (N\_CUHK405/20, 24108820, 14106622, 14110923, C4002-20W, C4002-21EF, C4033-19E) and the Chinese University of Hong Kong (CUHK) Research Committee to X.Z. We also acknowledge the support of the 2022 Guangdong–Hong Kong–Macao Greater Bay Area Exchange Programs of the SCNU.

## Author contributions

X.L., J.L., and C.G. designed the project; X.L., J.L., K.C., L.F., Y.L., Z.Y., C.L., J.Z., W.S., and H.L. performed the experiments; X.L., J.L., K.C., L.F., J.Z., W.S., H.L., C.Y., X.Z., and C.G. analyzed the results; X.L., J.L., C.G. wrote and/or edited the manuscript.

## Competing interests

The authors declare no competing interests.

## Additional information

**Supplementary information** The online version contains supplementary material available at <https://doi.org/10.1038/s41467-024-55292-w>.

**Correspondence** and requests for materials should be addressed to Caiji Gao.

**Peer review information** *Nature Communications* thanks Amélie Bernard, and the other, anonymous, reviewers for their contribution to the peer review of this work. A peer review file is available.

**Reprints and permissions information** is available at <http://www.nature.com/reprints>

**Publisher's note** Springer Nature remains neutral with regard to jurisdictional claims in published maps and institutional affiliations.

**Open Access** This article is licensed under a Creative Commons Attribution-NonCommercial-NoDerivatives 4.0 International License, which permits any non-commercial use, sharing, distribution and reproduction in any medium or format, as long as you give appropriate credit to the original author(s) and the source, provide a link to the Creative Commons licence, and indicate if you modified the licensed material. You do not have permission under this licence to share adapted material derived from this article or parts of it. The images or other third party material in this article are included in the article's Creative Commons licence, unless indicated otherwise in a credit line to the material. If material is not included in the article's Creative Commons licence and your intended use is not permitted by statutory regulation or exceeds the permitted use, you will need to obtain permission directly from the copyright holder. To view a copy of this licence, visit <http://creativecommons.org/licenses/by-nc-nd/4.0/>.

© The Author(s) 2024